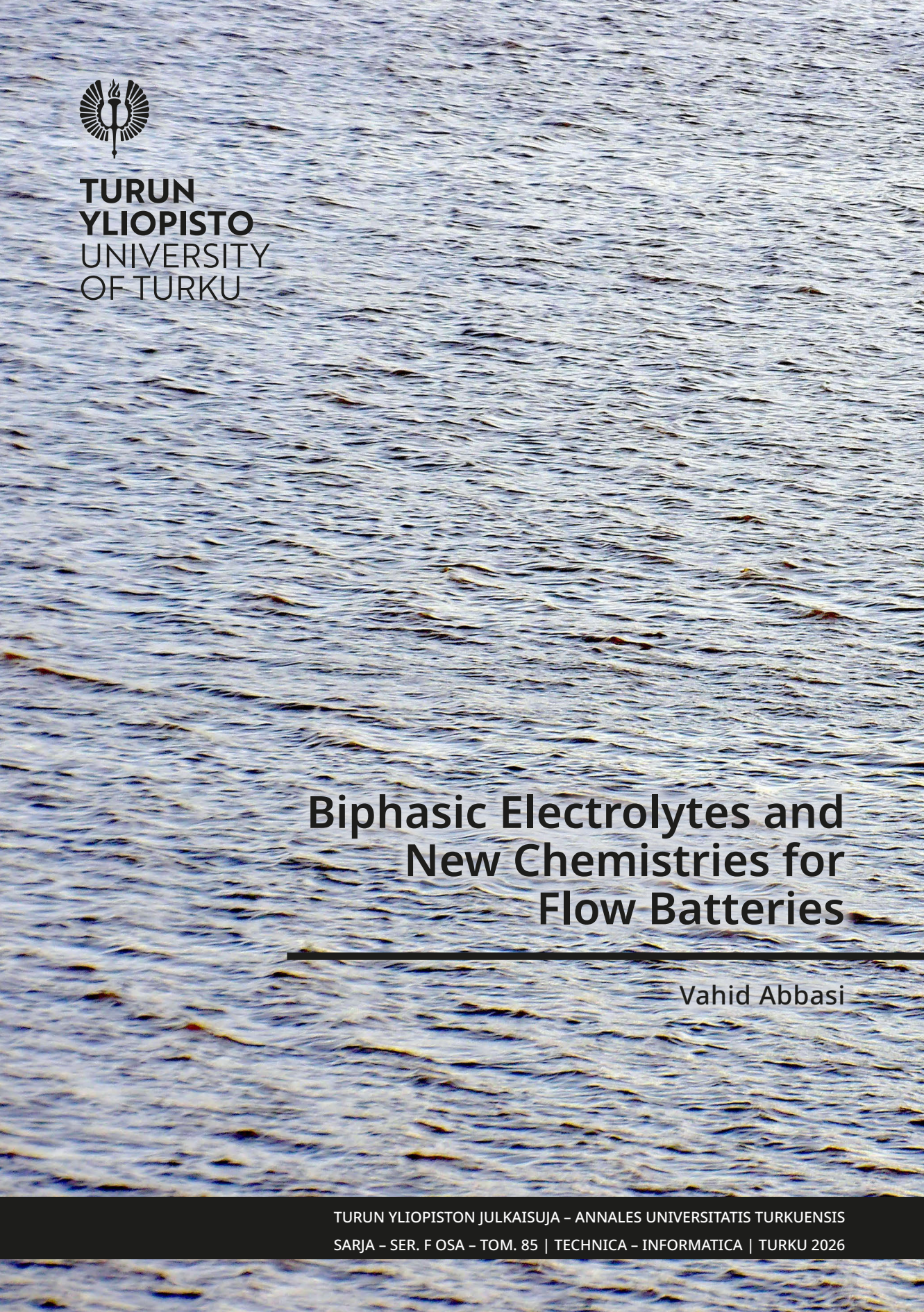

TURUN YLIOPISTO
UNIVERSITY OF TURKU

Biphasic Electrolytes and New Chemistries for Flow Batteries

Vahid Abbasi

TURUN YLIOPISTON JULKAISUJA – ANNALES UNIVERSITATIS TURKUENSIS
SARJA – SER. F OSA – TOM. 85 | TECHNICA – INFORMATICA | TURKU 2026

TURUN
YLIOPISTO
UNIVERSITY
OF TURKU

BIPHASIC ELECTROLYTES AND NEW CHEMISTRIES FOR FLOW BATTERIES

Vahid Abbasi

TURUN YLIOPISTON JULKAISUJA – ANNALES UNIVERSITATIS TURKUENSIS
SARJA – SER. F OSA – TOM. 85 | TECHNICA - INFORMATICA| TURKU 2025

University of Turku

Faculty of Technology
Department of Mechanical and Materials Engineering
Materials Engineering
Doctoral programme in Technology (DPT)

Supervised by

Professor Pekka Peljo
University of Turku
Turku, Finland

Dr. Eduardo Martínez González
Aalto University
Espoo, Finland

Reviewed by

Senior Researcher Rebeca Marcilla
IMDEA Energy Institute
Móstoles, Spain

Professor Imren Hatay Patir
Selcuk University
Konya, Turkey

Opponent

Professor Robert Dryfe
University of Manchester
Manchester, England

Cover Image: Vahid Abbasi

ISBN 978-952-02-0697-0 (PRINT)
ISBN 978-952-02-0698-7 (PDF)
ISSN 2736-9390 (Painettu/Print)
ISSN 2736-9684 (Sähköinen/Online)
Painosalama, Turku, Finland 2026

To the blood of those who walked the path of freedom

UNIVERSITY OF TURKU
Faculty of Technology
Department of Mechanical and Materials Engineering
Materials Engineering
VAHID ABBASI: Biphasic electrolytes and new chemistries for flow batteries
Doctoral Dissertation, 168 pp.
Doctoral Programme in Technology (DPT)
June 2026

ABSTRACT

Climate change demands immediate action to reduce our carbon footprint across all sectors. The rapid expansion of renewable energy sources like solar and wind power has created significant challenges for grid management due to their inherent intermittency. Energy storage systems have transitioned from powering consumer devices to serving as critical components that stabilize these variable renewable electricity supplies. Flow batteries stand out among competing technologies due to their ability to independently scale power and energy capacity, offering remarkable design flexibility for diverse applications. Vanadium-based electrolyte solutions have led the commercial market so far, yet their economic limitations and supply chain vulnerabilities have spurred investigation into alternatives.

This study explores biphasic solvent systems in flow battery applications and presents molecular candidates to replace conventional vanadium-based electrolytes. Biphasic configurations offer several operational advantages, including enhanced cell voltage when appropriate solvents are employed, alongside the use of organic solvents that facilitate access to solubilize more redox species. Microemulsion formation represents a particularly advantageous phenomenon in these systems, as addition of aqueous phase to the organic solvent increased both conductivity and stability of the flow battery electrolyte in battery.

This study further investigated a novel molecular system engineered as a high-performance alternative to conventional vanadium electrolytes, specifically tailored for operation in alkaline pH conditions. Within this media, we propose lithium chloranilate as the active species. This compound operates via a two-electron redox mechanism, enabling to achieve competitive energy densities essential for practical storage applications. Moreover, the capacity fade in this system could be recovered electrochemically in certain condition.

KEYWORDS: flow batteries, biphasic system, organic redox molecule, microemulsion

TURUN YLIOPISTO
Teknillinen Tiedekunta
Kone- ja materiaalitekniikan laitos
Materiaalitekniikka
VAHID ABBASI: Kaksifaasielektrolyytit ja uudet kemiat virtausakuissa
Väitöskirja, 168 s.
Teknologian tohtoriohjelma (DPT)
Kesäkuu 2026

TIIVISTELMÄ

Ilmastonmuutos vaatii välittömiä toimia hiilijalanjälkemme pienentämiseksi kaikilla sektoreilla. Uusiutuvien energialähteiden, kuten aurinko- ja tuulivoiman, nopea laajentuminen on luonut merkittäviä haasteita verkonhallinnalle niille ominaisen epäsäännöllisyyden vuoksi. Energian varastointijärjestelmät ovat siirtyneet kuluttajalaitteiden virtalähteistä kriittisiksi komponenteiksi, jotka vakauttavat näitä vaihtelevia uusiutuvan sähkön tarjontoja. Virtausakut erottuvat kilpailevien teknologioiden joukosta kykynsä ansiosta skaalata teho- ja energiakapasiteettia toisistaan riippumattomasti, tarjoten merkittävää suunnittelufleksibiliteettia erilaisiin sovelluksiin. Vanadiinipohjaiset elektrolyyttiliuokset ovat tähän asti johtaneet kaupallisia markkinoita, mutta niiden taloudelliset rajoitukset ja toimitusketjun haavoittuvuudet ovat kannustaneet vaihtoehtojen tutkimiseen.

Tässä tutkimuksessa tarkastellaan kaksivaiheiset liuotinjärjestelmiä virtausakkusovelluksissa ja esitetään molekyyliehdokkaita korvaamaan tavanomaiset vanadiinipohjaiset elektrolyytit. Kaksivaiheisilla konfiguraatioilla on useita toiminnallisia etuja, kuten parannettu kennojännite sopivien liuottimien käytön myötä sekä orgaanisten liuottimien käyttö, joka helpottaa useampien redoksilajien liuottamista. Mikroemulsion muodostuminen on näissä järjestelmissä erityisen edullinen ilmiö: vesifaasin lisääminen orgaaniseen liuottimeen paransi elektrolyytin sekä johtavuutta että stabiilisuutta akussa.

Tutkimuksessa tarkasteltiin lisäksi uudenlaista molekyylijärjestelmää, joka on suunniteltu korkean suorituskyvyn vaihtoehdoksi tavanomaisille vanadiinielektrolyyteille ja on erityisesti räätälöity toimimaan emäksisissä pH-olosuhteissa. Tässä väliaineessa ehdotamme aktiiviseksi lajiksi litiumkloranilaattia. Tämä yhdiste toimii kaksielektronisen redoksimekanismin kautta, mahdollistaen käytännön varastointisovelluksille välttämättömien kilpailukykyisten energiatiheyksien saavuttamisen. Lisäksi järjestelmän kapasiteetin heikkeneminen voitiin tietyissä olosuhteissa palauttaa sähkökemiallisesti.

AVAINSANAT: virtausakut, bifaasinen järjestelmä, orgaaninen redoksimolekyyli, mikroemulsio

Table of Contents

Abbreviations

ABS	aqueous biphasic systems
AOFB	aqueous organic flow batteries
Ag/AgCl	silver/silver chloride electrode
CC	constant current
CCCV	constant current–constant voltage
CE	coulombic efficiency
CV	constant voltage, or cyclic voltammetry or cyclic voltammogram
DCE	1,2-Dichloroethane
DME	1,2-Dimethoxyethane
DMFc	decamethylferrocene
EC	ethylene carbonate
EE	energy efficiency
EMC	ethyl methyl carbonate
Fc	ferrocene
HLB	hydrophile-lipophile balance
HLD	hydrophilic-lipophilic deviation
I	current
ITIES	interface between two immiscible electrolyte solutions
LiTB	lithium tetrakis(pentafluorophenyl)borate ethyl etherate
NMR	nuclear magnetic resonance
OCP	open circuit potential
OCV	open circuit voltage
PC	propylene carbonate
PDS	potential determination salt
SHE	standard hydrogen electrode
SOC	state of charge
TFT	trifluorotoluene
UV-Vis	ultraviolet-visible
VE	voltage efficiency
VFB	vanadium flow battery

List of Original Publications

This dissertation is based on the following original publications, which are referred to in the text by their Roman numerals:

I **Vahid Abbasi** and Pekka Peljo. Boosting the cell voltage in biphasic flow batteries via Galvani potential difference. *Phys. Chem. Chem. Phys.*, 2024; 26: 17476–17480.
https://doi.org/10.1039/D4CP01402B

II **Vahid Abbasi**, Ali Tuna, Eduardo Martínez González, Katarzyna Dusiło, Jose A. Manzanares, Marcin Opałło, Pekka Peljo. Exploring Galvani Potential Difference in Microemulsion-Based Flow Battery Systems. *Submitted*

III Ali Tuna[1], **Vahid Abbasi**[1], Carita Kvarnström, Pekka Peljo. Unveiling novel capacity (electro)recovery for Chloranilate-based alkaline redox flow batteries. *Journal of Electroanalytical Chemistry*, 2025; 11908.
https://doi.org/10.1016/j.jelechem.2025.119081

Contribution Statement

Doctoral candidate's role in Publication I-III:
• Research design: Participated in conceptualization and methodology design.
• Laboratory work: Conducted investigations and experimental work.
• Data processing: Performed formal analysis, validation, and visualization of results.
• Writing of the manuscript: Wrote the original draft (Publication I and II) and contributed to review and editing (Publication I–III).

Declaration of AI use

In preparing this dissertation, generative artificial intelligences (AI) (Claude and ChatGPT) have been used as a search engine and proofreader. Research questions, data analysis and conclusions were developed without AI.

1 Introduction

The world is facing serious environmental problems such as air pollution, rising temperatures, and extreme weather events are becoming more common and more dangerous. Much of this damage comes from burning fossil fuels like coal, oil, and gas, which release harmful greenhouse gases into the atmosphere. Many countries are working on an energy transition by shifting from dirty, polluting energy sources to clean, renewable ones like solar, wind, and hydropower. This transition is not just about technology, it also involves changing laws, updating infrastructure, and helping people adapt. A fair and successful energy transition means that all countries share the same climate goals while having the freedom to chart their own paths forward based on their available resources, capabilities, and local circumstances, creating a collaborative global effort where different approaches work together toward the common aim of a sustainable future.

Integrating renewable energy electricity sources like solar and wind into existing power systems presents significant challenges due to their intermittent nature, as availability of sunlight and wind availability fluctuate, often unpredictably. Maintaining grid stability requires advanced energy storage solutions and demand management strategies that can balance supply and demand in real time. This necessitates substantial infrastructure investment, including smart grid technologies, large-scale battery systems, and dispatchable backup generation capable of rapid response. Enhanced forecasting models are equally critical for anticipating renewable output and optimizing grid operations. Without comprehensive planning and coordination, energy systems risk inefficiency, curtailment, or supply disruptions. By advancing both technological capabilities and infrastructure development, we can establish energy systems that are not only cleaner and more resilient but also adaptable to evolving energy demands and climate realities.

1.1 Thesis outline

This thesis is organized into 8 chapters, each addressing a key component of developing novel electrolyte systems for flow battery applications.

Chapter 1. Introduction

This chapter introduces the broader context of the energy transition, establishing the motivation for large-scale energy storage and making the case for the accelerated adoption of renewable energy sources as an essential response to climate change.

Chapter 2. Background

This chapter provides a comprehensive overview of existing energy storage technologies, followed by a detailed discussion of flow battery systems and their classifications and configurations.

Chapter 3. Biphasic systems

This chapter discusses biphasic solvent systems and the effect of the Galvani potential difference on cell voltage, followed by an overview of microemulsion principles and a review of microemulsion-based flow battery systems.

Chapter 4. Contextualization and Research Objectives

This chapter provides a clear framework connecting the two main research directions of the thesis by defining the scientific context, objectives, and key challenges in both biphasic/microemulsion electrolytes and new flow battery chemistries. It serves as a bridge between the background and the methodological and results chapters by clarifying the rationale and structure of the work.

Chapter 5. Experimental Technics

This chapter provides an overview of the electrochemical and spectroscopic techniques utilized in this work, establishing the theoretical and methodological foundation for the experimental investigations presented in subsequent chapters. The fundamental operating principles of each technique are described, along with a discussion of the specific information they provide in the context of electrolyte characterization and flow battery performance evaluation.

Chapter 6. Materials and Methods

This chapter presents the chemicals, materials, and instrumentation used in this thesis, along with a detailed description of the preparation procedure for the microemulsion electrolyte, covering the key parameters and conditions required to achieve stable and reproducible formulations suitable for flow battery applications.

Chapter 7. Biphasic systems in Flow Batteries

This chapter presents the findings of Publications I and II, discussing the development and characterization of biphasic and microemulsion-based flow battery systems, with a particular focus on investigation of the Galvani potential difference and its influence on cell performance.

Chapter 8. Investigation of new materials

This chapter presents the investigation of a new water-soluble electroactive molecule for preparing alkaline flow battery negolyte, describing its electrochemical performance and flow battery operation, and specific conditions for its capacity recovery.

Chapter 9. Conclusion and Outlook

This chapter summarizes the key findings of this thesis, drawing overarching conclusions from the investigations conducted across all preceding chapters, and outlines promising directions for future research in biphasic and microemulsion-based flow battery systems and novel organic electrolyte development.

2 Background

This chapter starts with brief introduction of the main energy storage technologies. Then comprehensive discussion of the different flow battery types is presented, beginning with commercially mature technologies such as vanadium and zinc-bromine systems, and progressing toward emerging configurations that have gained considerable attention in recent research, including aqueous organic and organic solvent-based flow batteries.

2.1 Energy storage systems

Produced energy can be stored using various methods and at different scales. Mechanical storage options include pumped hydro storage, compressed air energy storage, and flywheel systems. Thermal storage technologies encompass molten salt systems, phase change materials, and innovative sand-based storage solutions. However, recent research has highlighted electrochemical energy storage as a promising approach. This category includes supercapacitors and various battery types such as lithium-ion, sodium-ion, lead-acid, and flow batteries.[1]

Batteries have emerged as the most popular energy storage systems due to their versatility in both portable and stationary applications. They excel in short- to medium-term storage scenarios and can be readily integrated with electricity generators. Their rapid response times and ability to be deployed in hybrid configurations make them particularly attractive for diverse energy storage needs.[2]

Among all battery technologies, flow batteries offer distinctive properties that make them suitable for numerous applications. Flow batteries store energy through reduction-oxidation reactions of electroactive species dissolved in liquid electrolytes rather than within solid electrodes.[3] The electrolytes are housed in separate external tanks, while the electrochemical reactions occur in a central stack where the two electrolytes flow through, separated by an ion-selective membrane. This innovative design provides significant advantages: increasing tank size (and thus electrolyte volume) directly increases energy storage capacity, while adding more stacks enhances power output. Beyond this exceptional scalability, flow batteries can have an impressive operational lifetime exceeding 25 years. Some possible applications

could be for example grid stabilization and peak shaving, renewable energy integration, remote and off-grid applications, and industrial load management.[4]

2.2 Flow batteries

Vanadium flow batteries (VFBs) utilize vanadium ions in different oxidation states as the active species in both positive and negative electrolytes.[5] This configuration eliminates the cross-contamination issues that plague other flow battery chemistries, as both sides contain the same base element in different oxidation states. VFBs demonstrate exceptional cycle stability, with systems capable of performing thousands of deep discharge cycles while experiencing minimal capacity degradation, making them ideal for long-term, grid-scale energy storage applications.[6,7]

However, while vanadium flow batteries are the most commercialized chemistry, they face several significant drawbacks. The vanadium market presents supply chain challenges, as the primary mining operations are concentrated in China, Russia, South Africa, and Brazil, with no substantial sources within the European Union.[8] Additionally, the electrolyte consists of concentrated sulfuric acid, which is highly corrosive, and vanadium itself is toxic to aquatic life, raising environmental and safety concerns.[9] Furthermore, the vanadium used in flow batteries must maintain exceptional purity; otherwise, accumulated impurities can disrupt normal operation and obstruct electrolyte flow during 10-15 years of use. Due to these limitations, research groups worldwide are actively seeking to replace vanadium with more cost-effective, safer, and readily available materials.[10] Figure 1 shows the schematic structure of vanadium flow battery.

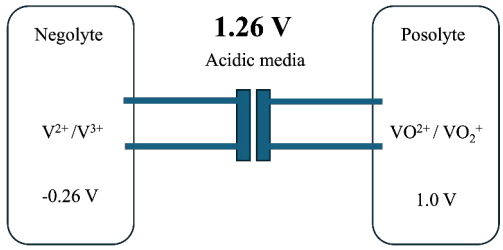

Figure 1. Structure of vanadium flow battery.

In recent years, alternative technologies such as zinc-bromine, iron-chromium, iron-based, copper-based, and organic flow batteries have emerged through start-ups and established companies, all competing to capture market share in the evolving energy storage landscape.[11]

Copper-based or iron-based batteries are using the metal in different oxidation numbers in posolyte and negolyte. For example, a copper-based flow battery is considered promising for large-scale energy storage owing to copper's abundance, relatively low cost, and favourable electrochemical properties. In such batteries, copper typically undergoes redox reactions between Cu^{2+}/Cu^{+} and Cu^{+}/Cu^{0} states within aqueous electrolytes, often separated by an ion-exchange membrane. Some designs involve direct electrodeposition of metallic copper during charging, while others pair copper with another redox couple such as iron or zinc.[12] Despite their potential, copper-based flow batteries face challenges such as copper dendrite formation, limited cycle life due to electrode degradation, and electrolyte instability, all of which hinder their long-term performance and scalability for practical applications. Most copper-based flow batteries operate at cell potentials between 0.6 V and 1.2 V[13]. Figure 2 shows the schematic and working potential of copper-based and iron-based flow batteries.

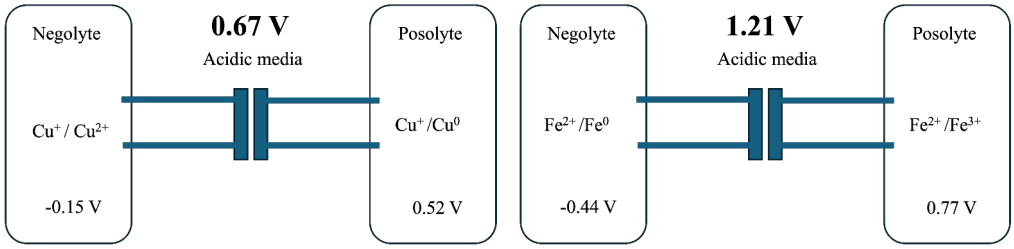

Figure 2. Structure of copper-based (left) and iron based (right) flow battery.

A zinc–bromine flow battery is a hybrid flow battery in which energy is stored via the reversible reactions of zinc and bromine: during charging, Zn^{2+} is reduced and plated as metallic Zn on the negative electrode, while Br^{-} is oxidized to Br_2 (often complexed as polybromides) at the positive electrode; on discharge, the processes reverse. In practice, zinc–bromine flow battery can reach a nominal open-circuit voltage of about 1.8 V under ideal conditions (Figure 3), which is very high for aqueous systems.[14,15] The system typically employs an aqueous $ZnBr_2$ electrolyte, sometimes complemented by complexing agents (e.g. quaternary bromide salts) to stabilize bromine and reduce its volatility and crossover. While zinc–bromine flow batteries promise advantages such as the use of earth-abundant elements, potentially high energy density, and safer aqueous operation compared to organic or lithium systems, they face several challenges, including zinc dendrite formation, uneven zinc deposition, hydrogen evolution, slow bromine redox kinetics, bromine crossover and volatility, high toxicity and corrosivity of gaseous Br_2 and electrode and membrane corrosion, all of which can reduce cycle life and overall system efficiency.[15]

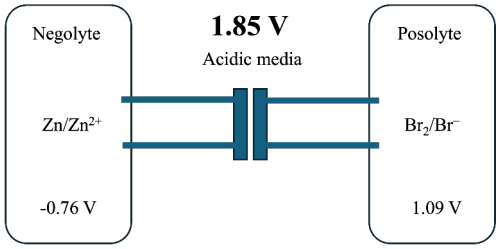

Figure 3. Structure of Zn-Br flow battery.

An iron–chromium flow battery is one of the earliest and most studied flow battery systems, operating through the reversible redox reactions of iron and chromium ions in aqueous acidic electrolytes. [16,17]During charging, Fe^{2+} is oxidized to Fe^{3+} at the positive electrode, while Cr^{3+} is reduced to Cr^{2+} at the negative electrode; these reactions reverse during discharge. as shown in Figure 4, the overall cell reaction produces an open-circuit voltage of about 1.18 V under standard conditions. Both active species are derived from abundant and low-cost materials, making Fe–Cr batteries attractive for large-scale, long-duration energy storage. The system also benefits from excellent chemical stability and non-flammable aqueous electrolytes. However, its performance is limited by several issues, including slow kinetics of the Cr^{3+}/Cr^{2+} redox couple, hydrogen evolution at the negative electrode, electrolyte cross-contamination, and capacity decay over long cycling. [6]

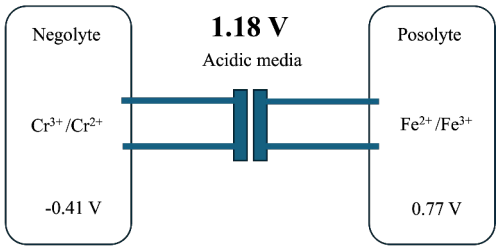

Figure 4. Structure of iron-chromium flow battery.

2.2.1 Aqueous organic flow batteries (AOFBs)

The investigation of new electrolyte materials has focused primarily on organic redox-active molecules and advanced metal coordination[18] complexes on developing as alternatives to conventional vanadium systems. Organic compounds such as quinones[19,20], viologens[21], TEMPO derivatives[22], and phenazine-based molecules[23] could offer significant advantages including earth abundance, tunable redox potentials, and reduced environmental impact. Researchers have made substantial progress in addressing early limitations of organic electrolytes, particularly

improving their aqueous solubility and cycling stability through strategic functionalization. For instance, modified anthraquinones[24,25] have demonstrated excellent long-term stability in alkaline solutions while maintaining high concentrations necessary for practical energy density. Beyond organics, metal coordination complexes based on iron[26], chromium[16], and zinc[27] are being explored for their cost advantages and performance characteristics. Ligand engineering has emerged as a powerful strategy to prevent crossover, enhance stability, and optimize redox potentials, with chelating agents and custom-designed ligands fundamentally altering the electrochemical behavior of metal centers. Some of common organic structures used in flow batteries are shown in Figure 5.

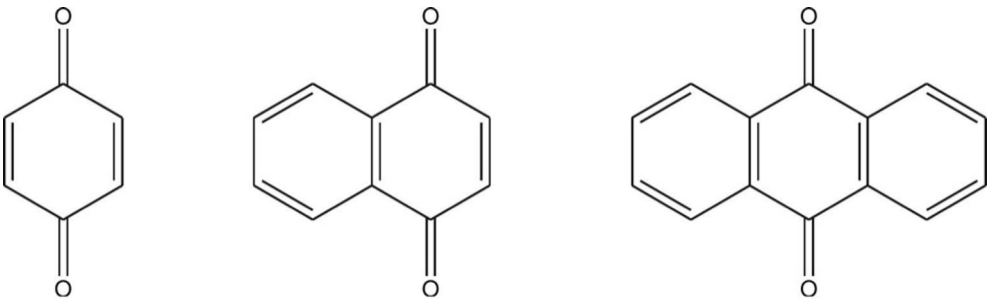

Figure 5. Chemical structures of 1,4-benzoquionone (left), 1,4-naphthaquinone (middle), and 9,10-anthraquionone (right).

Table 1 shows several examples of aqueous organic flow batteries (AOFBs), highlighting a critical constraint common to their design: their practical cell potential is fundamentally capped at approximately 1.6 to 1.7 V. This voltage ceiling arises not from the organic molecules themselves but from the electrochemical stability window of the aqueous electrolyte, primarily water. When the charging potential exceeds this threshold, the desired oxidation of the organic active material is outcompeted by the thermodynamically favourable oxygen/hydrogen evolution reaction (OER/HER), where water is electrolyzed to form gas at the electrode.[28] These parasitic reactions not only wastes input energy and reduces efficiency but can also degrade the electrolyte and compromise system safety. Therefore, the development of AOFBs focuses on designing robust organic molecules that operate efficiently within this narrow electrochemical window to ensure long-term, stable cycling.

Table 1. Aqueous organic flow batteries examples.

Negolyte	Posolyte	OCP (V)	Capacity Utilization*	Capacity Decay**	Cycle	Ref
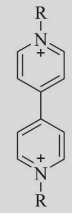 (SPr)2V 0.25 M in 4.0 M LiTFSI	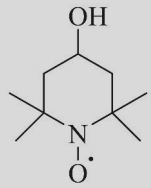 4-Hydroxy-TEMPO 0.5 M in 4.0 M LiTFSI	1.08	69%	0.048% /cycle 0.60 %/day	285	29
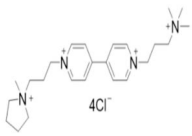 [PyrTMAV]Cl_4 0.5 M in 2.0 M NaCl	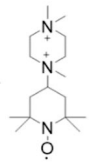 TMP-TEMPO 1.0 M in 2.0 M NaCl	1.58	90%	0.17% /cycle 0.9 % /day	176	30
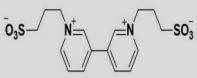 SPr-Bpy 1.2 M in 1.2 M NaCl and 0.4 M CH_3CO_2Na	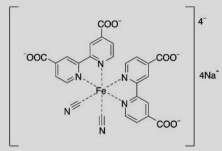 $Na_4[FeII(Dcbpy)_2(CN)_2]$ 1.02 M in 0.1 M NaOH	1.2	73%	0.1% / cycle 2.3% / day	250	31
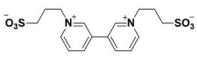 $(SPr)_2$ V 0.1 M in 1.0 M NaCl	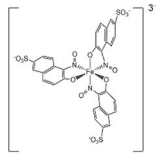 NGB 0.1 M / HP-β-CD 0.2 M in 1.0 M NaCl	1.22	21%	0.008% / cycle	250	32
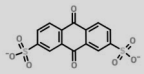 2,7-AQDS 0.2 M in 0.5 M Na_2SO_4	 HQS 0.2 M in 0.5 M Na_2SO_4	0.83	70%	No data	120	33

Negolyte	Posolyte	OCP (V)	Capacity Utilization*	Capacity Decay**	Cycle	Ref
 DHBQ 0.5 M in 1.0 M KOH	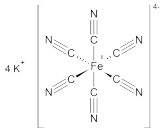 $K_4Fe(CN)_6$ 0.4 M in 1.0 M KOH	1.21	60%	0.8% / cycle	50	34
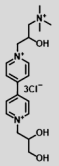 Dex-DiOH-Vi 2.5 M in pure water	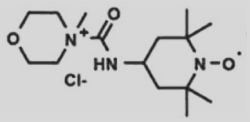 MMA-TEMPO 2.5 M in pure water	1.09	89.9%	~0% / 14 days	250	35
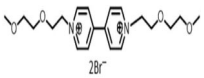 Vi-OEG$_3$ 0.5 M in 2.0 M NaBr	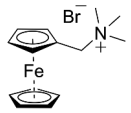 FcNEBr 0.5 M in 2.0 M NaBr	0.95	95%	0.0001%/ cycle 0.0025% / day	138	36
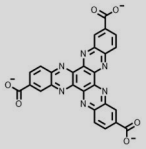 HATNTA 0.25 M in 0.5 M KOH	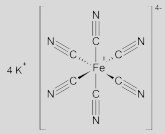 $K_4Fe(CN)_6$ 0.25 M in 0.5 M KOH	1.24	94.2%	0.021% cycle / 0.168% / day	80	37
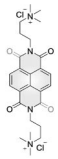 NDI 0.1 M in 2.0 M NaCl	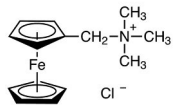 FcNCl 0.5 M in 2.0 M NaCl	1.07	82.4%	0.004% /cycle 0.52% / day	100	38

Negolyte	Posolyte	OCP (V)	Capacity Utilization*	Capacity Decay**	Cycle	Ref
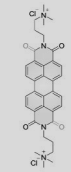 PDI 0.02 M in 2.0 M NaCl	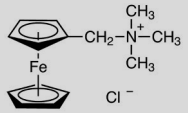 FcNCl 0.02 M in 2.0 M NaCl	1.06	89.72%	0.0004% /cycle 0.1% / day	1000 0	[38]
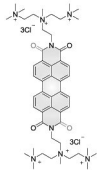 TPDI 0.05 M in 2.0 M NaCl	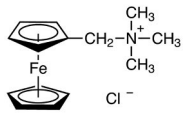 FcNCl 0.05 M in 2.0 M NaCl	0.96	87.17%	0.002 %/ cycle 0.39% / day	560	[38]

*Battery capacity utilization represents the extent to which a battery's stored energy is discharged relative to its maximum storage capability. **Battery capacity decay (or fade) is the irreversible, gradual decrease in a rechargeable battery's ability to store energy over time and usage cycles.

2.2.2 Organic solvent-based flow batteries

One of the most compelling aspects of organic solvent-based flow batteries is precisely their broad electrochemical stability window, which offers high operational voltages.[39] This elevated cell potential is a key factor in overcoming one of their primary challenges.[40] While nonaqueous systems often contend with lower conductivity, higher viscosity, and material compatibility issues, all of which can reduce power density and increase system cost, the significantly higher voltage window directly compensates for these limitations by enabling a substantially higher energy density.[42] Therefore, the core trade-off becomes a balance between achieving greater energy storage per unit volume and managing the power and engineering complexities associated with organic electrolytes. Research focuses on designing new organic molecules that are highly soluble and stable in these systems to fully leverage this high-voltage advantage, making it a fundamental driver for their development. Table 2. contains some examples of organic solvent-based electrolyte flow batteries.

Table 2. Organic solvent-based electrolyte flow batteries.

Negolyte	Posolyte	OCP (V)	Capacity Utilization	Capacity Decay/Cycle	Cycles	Ref
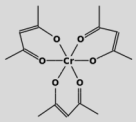 $Cr^{III}(acac)_3$ 0.4M In 0.5 M $TEABF_4$ in CH_3CN	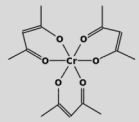 $Cr^{III}(acac)_3$ 0.4 M In 0.5 M $TEABF_4$ in CH_3CN	3.4	No data	No data	10	[43]
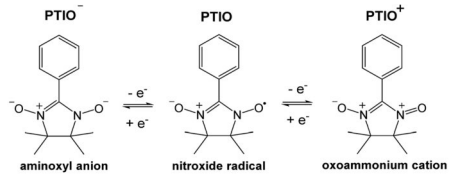 0.5 M concentration In 1.0 M $TBAPF_6$/ CH_3CN		1.73	43%	No data	15	[44]
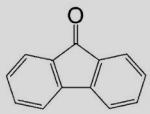 0.1 M concentration in 1 M TEA-TFSI/DME	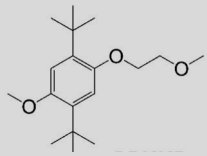 0.1 M concentration in 1 M TEA-TFSI/DME	2	No data	0.2 %	50	[45]
Li foil	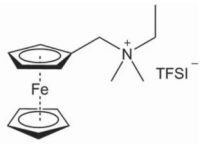	3.49	No data	0.05 %	100	[46]
1.2 M LiTFSI in EC/PC/EMC	1.7 M in 1.2 M LiTFSI in EC/PC/EMC					

3 Biphasic System

This chapter begins with an introduction to biphasic systems and the concept of the Galvani potential difference at liquid–liquid interfaces. Subsequently, electrochemical systems relevant to biphasic environments, such as membrane-less flow batteries, are presented. Finally, microemulsion systems are discussed.

Conventional water-based batteries utilize a single aqueous electrolyte solution where all electroactive species are dissolved and operate within the same chemical environment.[47,48] Biphasic flow batteries represent an innovative departure from this design by utilizing two immiscible liquid phases, typically an aqueous phase paired with an organic solvent phase, or two immiscible aqueous phases that coexist within the same electrochemical cell. In these systems, distinct liquid regions that do not mix are maintained, for example like how oil and water separate into layers. Each phase can host different redox active molecules tailored to its chemical environment: water soluble compounds in the aqueous phase and organic soluble compounds in the organic phase.[49]

Aqueous biphasic systems (ABS) are ternary systems formed by water and two water-soluble compounds, such as two polymers, a polymer and a salt, two salts, an ionic liquid and a salt, or an ionic liquid and a polymer, which form two distinct aqueous phases above given concentrations of phase-forming components where both phases contain water. These systems are particularly valuable because the selective enrichment of molecules in each aqueous phase allows for separation driven by the intrinsic immiscibility of the two liquid phases rather than by expensive physical membranes. The partition coefficients of active molecules between the two phases determine the degree of separation and cross-contamination. [50,51] However, in conventional flow battery cell with biphasic systems, an ion- selective membrane is still often necessary, as even porous membranes cannot fully prevent phase mixing. Due to these persistent challenges, the integration of a membrane remains a practical requirement for ensuring long-term, stable operation.[52]

3.1 Galvani potential difference in biphasic systems

Water-based flow batteries face several inherent limitations, including a narrow electrochemical potential window and low solubility for organic compounds. Organic solvents offer a broader potential window and can dissolve a wider variety

of electroactive compounds, making them a prominent focus in current research. Additionally, flow batteries can utilize hybrid systems that combine organic solvents and aqueous solutions in separate tanks.[51,53] When implementing these hybrid organic/aqueous systems, specific physicochemical properties must be carefully considered, particularly at the membrane interface within the cell stack where the electrolytes meet to facilitate ion transfer during charging and discharging cycles.[54]

Through careful solvent selection, one particularly valuable physicochemical property that can be exploited in flow batteries is the Galvani potential difference. [55] The Galvani potential difference is a fundamental electrochemical phenomenon that has been recognized since the 1970s,[56,57] occurring at the interface between two immiscible electrolyte solutions. When two liquids that do not mix, such as water and an organic solvent come into contact, they form a boundary where ions and other charged species can distribute themselves between the two phases. This distribution is not random; rather, it creates an electrical potential difference across the interface that can be remarkably large, reaching values of up to 0.7 volts.[58] This potential arises from the unequal partitioning of ions between the two phases, with each phase preferentially attracting or repelling certain ionic species based on their chemical properties and solvation energies.[59] The interface essentially acts like a charged boundary layer, with one phase becoming slightly more positive and the other more negative relative to each other.[60,61]

As an example, by adding a potential determining salt (PDS) such as lithium tetrakis(pentafluorophenyl)borate ethyl etherate (LiTB), which contains a hydrophilic cation and a hydrophobic anion, to two immiscible solvents, the ions partition themselves at the interface between the two immiscible electrolyte solutions (ITIES) upon reaching equilibrium.[62,63] This partitioning creates a charged interface, and the resulting potential difference at the ITIES constitutes the Galvani potential difference, which can be simply represented at the electrolyte-electrolyte interface as shown in Figure 6.

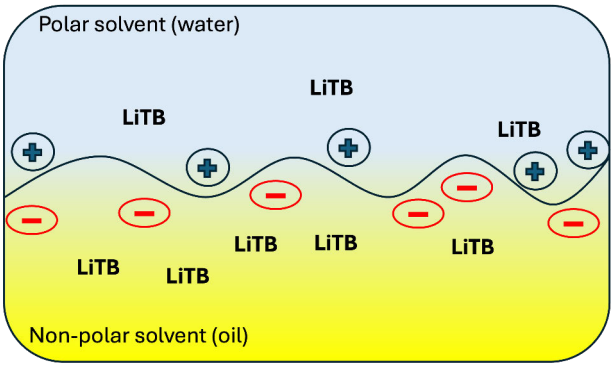

Figure 6. Polarized interface at ITIES.

Even nominally non-polar organic solvents possess a finite relative permittivity, which directly controls the thickness of the diffuse double layer at their interface with water. For solvents with a very low relative permittivity, such as TFT ($\varepsilon_r \approx 9.2$)[64] or DCE ($\varepsilon_r \approx 10.3$)[65], the organic-side diffuse layer capacitance is small, and since the total interfacial capacitance is a series combination of the two back-to-back diffuse layers, most of the Galvani potential difference drops on the organic side, producing a sharp, strongly polarized interface. For solvents with a higher relative permittivity, such as propylene carbonate ($\varepsilon_r \approx 65$)[66], the organic-side diffuse layer is thicker and its capacitance is closer in value to the aqueous side, so the Galvani potential difference is distributed more evenly, the interfacial electric field is weaker, and the two solvents can mix more at the boundary.[67] In a conventional single-phase (water as solvent in both posolyte and negolyte) flow battery, the cell potential during discharge is determined by the difference between the cathode and anode redox potentials:[68]

$$V_{\text{battery}} = E^0_{\text{cathode}} - E^0_{\text{anode}} \quad (1)$$

where E^0_{cathode} and E^0_{anode} are the standard reduction potentials of the posolyte and negolyte redox couples. For typical aqueous redox flow batteries, this relationship is straightforward as both half-cell reactions occur in the same solvent environment with similar solvation energetics. The theoretical voltage is simply the difference between the two redox potentials measured against a common reference electrode.
When a biphasic organic/aqueous interface is incorporated into the battery architecture, an additional Galvani potential difference ($\Delta_o^w \phi$) contributes to the overall cell voltage. The modified cell potential becomes: [55]

$$V_{\text{battery}} = E^0_{\text{cathode}} - E^0_{\text{anode}} + \Delta_o^{\text{w}} \phi \quad (2)$$

According to the electrochemistry textbooks[69,70], Galvani potential of the phase ϕ is defined as the sum of the outer potential ψ and inner potential χ, $\phi = \chi + \psi$ and it is included in the expression of the electrochemical potential of the species $\tilde{\mu}_i = \mu_i + z_i F \phi_i$, where $\tilde{\mu}_i$ is the chemical potential of the species *i*, *F* is the Faraday constant, and z_i is the charge of the species *i*.[71]Here, the chemical potential describes the energy of adding a species *i* to the phase, and $z_i F \psi_i$, is the electrostatic work to bring one mol of species *i* from vacuum to the surface of the phase and $z_i F \chi_i$, is the work to cross the interface of the phase with vacuum. Chemical potential is connected to the Gibbs free energy *G* by

$$\mu_i = \left(\frac{\partial G}{\partial N_i}\right)_{T,p,N_{j\neq i}} \quad (3)$$

where *N* is the number of particles. If temperature *T* and pressure *p* are constant, change in the Gibbs free energy is

$$dG = \sum_{i=1}^{n} \mu_i dN_i \quad (4)$$

When species *i* is in equilibrium in two phases, electrochemical potential of the species *i* is equal. This section follows the description of refs.[61,72,73]

$$\tilde{\mu}_i^{\mathrm{w}} = \tilde{\mu}_i^{o} \tag{5}$$

$$\mu_i^{\mathrm{w}} + z_i F \phi_i^{\mathrm{w}} = \mu_i^{o} + z_i F \phi_i^{o} \tag{6}$$

$$\mu_i^{0,\mathrm{w}} + RT \ln a_i^{\mathrm{w}} + z_i F \phi_i^{\mathrm{w}} = \mu_i^{0,\mathrm{o}} + RT \ln a_i^{o} + z_i F \phi_i^{o} \tag{7}$$

$$\phi_i^{w} - \phi_i^{o} = \frac{\mu_i^{0,\mathrm{o}} - \mu_i^{0,\mathrm{w}}}{z_i F} + \frac{RT}{z_i F} \ln \frac{a_i^{o}}{a_i^{\mathrm{w}}} \tag{8}$$

Here, we can define the Galvani potential difference between aqueous and organic phases as $\Delta_o^{\mathrm{w}}\phi = \phi_i^{\mathrm{w}} - \phi_i^{o}$ and the standard Gibbs energy as $\Delta G_{\mathrm{tr},i}^{0,w\to o} = \mu_i^{0,\mathrm{o}} - \mu_i^{0,\mathrm{w}}$ resulting in the definition of the standard potential of ion transfer as:

$$\Delta_o^{w}\phi_i^{0} = \frac{\Delta G_{\mathrm{tr},i}^{0,w\to o}}{z_i F} = \frac{\mu_i^{0,\mathrm{o}} - \mu_i^{0,\mathrm{w}}}{z_i F} \tag{9}$$

where $\mu_i^{0,\,\alpha}$ is the standard chemical potential of *i* in either phase (α = o or w), z_i is the charge of *i*, and *F* is the Faraday constant. Equation (8) illustrates the connection between the Galvani potential difference and partition of ions, resulting in the Nernst equation for ion partition (analogous with metal electrodes): [74,75]

$$\phi^{w} - \phi^{o} = \Delta_o^{\mathrm{w}}\phi = \Delta_o^{\mathrm{w}}\phi_i^{0} + \frac{RT}{z_i F} \ln \frac{a_i^{o}}{a_i^{\mathrm{w}}} = \Delta_o^{\mathrm{w}}\phi_i^{0\,'} + \frac{RT}{z_i F} \ln \frac{c_i^{o}}{c_{\mathrm{i}}^{\mathrm{w}}} \tag{10}$$

where $\Delta_o^{w}\phi_i^{0\,'}$ is the formal potential of ion transfer for species *i* from water to oil, *R* is the molar gas constant, *T* is the temperature and a_{i} and c_{i} are the activity and concentration of species *i*, respectively.

3.2 Membrane less flow batteries

A key motivation behind biphasic and triphasic designs is the potential to eliminate the membrane, which is often an expensive component of conventional flow batteries. However, early biphasic systems faced considerable practical challenges. Complex cell geometries required to maintain stable liquid-liquid interfaces often led to problems like emulsification during pumping, high resistance, and difficulties with reversible ion transfer. These issues decrease the theoretical gains in efficiency and power density.[76,77]

Systems consist of two water-rich phases formed by combining water-soluble compounds such as ionic liquids with salts or polymers, creating a spontaneous liquid-liquid interface that physically separates redox-active species without requiring artificial barriers. [78] The selective partitioning of organic redox molecules between phases is governed by their partition coefficients, which determine their preferential distribution based on solubility differences. Pioneering work by Marcilla and colleagues demonstrated that redox-active organic molecules, such as methyl

viologen and 2,2,6,6-tetramethyl-1-piperidinyloxy (TEMPO), can be selectively enriched in each aqueous phase, enabling theoretical cell voltages as high as 1.6 V.[78] This approach not only reduces costs by eliminating expensive membranes but also maintains the advantages of aqueous electrolytes, avoiding toxic organic solvents and providing a more environmentally sustainable alternative to conventional vanadium-based redox flow batteries.

The electrochemical performance of membrane-free flow batteries has been significantly improved through optimized biphasic electrolyte design and advanced cell architectures. Recent flow reactor designs have successfully maintained interphase stability under dynamic flowing conditions, extending operation from static configurations to continuous cycling over extended periods. However it works just under low flow rates and low current densities, but these advances demonstrate that membrane-free systems can compete with conventional redox flow batteries via offering significant cost and sustainability advantages.[79]

Current research focuses on addressing remaining challenges to enable large-scale commercialization. The primary limitation is the relatively low concentration of active species (approximately 0.1 M) compared to vanadium systems (1.6 M), necessitating continued efforts to develop redox molecules with improved solubility and electrochemical stability at higher concentrations. Advanced analytical techniques including scanning electrochemical microscopy (SECM) have provided unprecedented insights into concentration gradients and crossover mechanisms at the liquid-liquid interphase, enabling quantification of self-discharge phenomena.[80,81] Computer-aided design approaches using conductor-like screening models are accelerating the discovery of optimized biphasic electrolyte compositions and active species pairs.[82] These developments position membrane-less flow batteries as viable candidates for large-scale stationary energy storage applications, particularly for grid-level renewable energy stabilization, with recent demonstration systems indicating movement toward market implementation within the near term.

3.3 Microemulsion systems

A microemulsion is a thermodynamically stable, isotropic liquid dispersion of two immiscible phases, typically water and oil, stabilized by an interfacial film of surfactant molecules, often with a co-surfactant. Its defining characteristic is spontaneous formation, requiring no high-energy input, and exceptional stability against phase separation.[83] This stability arises from achieving an ultra-low interfacial tension, which facilitates the formation of nanoscale domains (typically 10-100 nm). These domains are smaller than the wavelength of visible light, rendering the system optically transparent or translucent, a key distinguishing feature from conventional, milky macroemulsions.

The system comprises three essential components: a polar (aqueous) phase, a relatively less-polar (oily) phase, and surfactant, usually a co-surfactant like a short-chain alcohol can help the main surfactant. The surfactant, an amphiphile, is the primary stabilizer, while the co-surfactant modulates the interfacial film's flexibility and curvature. The precise ratio of these components determines the system's microstructure, which can exist in several equilibrium phases: oil-swollen micelles in water (o/w), water-swollen reverse micelles in oil (w/o), or a bicontinuous structure where both oil and water form continuous, interpenetrating nanoscale channels. This phase behavior is mapped and predicted using thermodynamic phase diagrams. A simple microemulsion phase diagram is shown at Figure 7.

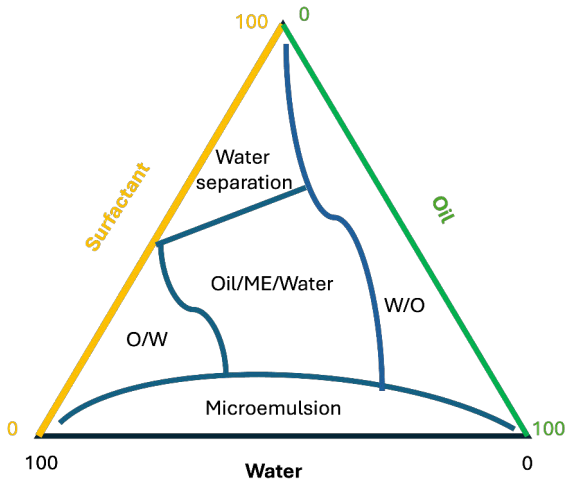

Figure 7. Example of a microemulsion phase diagram.

Surfactants are categorized by the nature of their hydrophilic head group into ionic (anionic, cationic, amphoteric) and nonionic types as shown in Figure 8. Selection is critically guided by the Hydrophile-Lipophile Balance (HLB) number, a semi-empirical scale (0-20) that quantifies a surfactant's relative affinity for oil or water. Low HLB values (1-9) indicate lipophilic surfactants suitable for w/o microemulsions, while high HLB values (11-20) denote hydrophilic surfactants that stabilize o/w systems. An intermediate HLB range (~9-12) is often associated with bicontinuous phases. Formulators frequently use surfactant blends to achieve an effective HLB value optimized for a specific oil, allowing precise control over the interfacial curvature and resulting nanostructure. [84]

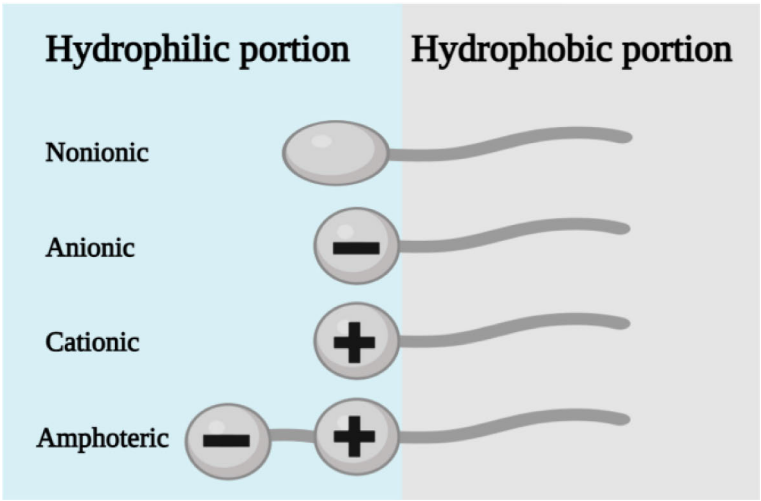

Figure 8. Different types of surfactants reproduced with permission Creative Commons Attribution (CC BY) license[84].

The phase behaviour of surfactant-oil-water systems is systematically classified by the Winsor scheme, which describes the equilibrium state between the microemulsion and excess bulk phases, as shown in Figure 9. The four primary Winsor types are defined by the number and nature of coexisting phases. A Winsor I system consists of an oil-in-water (o/w) microemulsion in equilibrium with an excess oil phase. Conversely, a Winsor II system features a water-in-oil (w/o) microemulsion in equilibrium with an excess water phase. The Winsor III, or "middle-phase," system is a three-phase equilibrium where a bicontinuous microemulsion, often possessing ultralow interfacial tension against both oil and water, coexists with separate excess oil and water phases; this state is particularly sought after in enhanced oil recovery.[85] Finally, the Winsor IV system represents a single-phase, optically isotropic microemulsion with no excess phases, which is the target for most formulation applications. Transitions between these states can be induced by formulation variables such as salinity, temperature, surfactant chemistry, and oil type, a concept formalized in the hydrophilic-lipophilic deviation (HLD) framework.

The functional properties of microemulsions enable broad applications across industries. They serve as advanced delivery vehicles in pharmaceuticals and cosmetics, as efficient carriers for pesticides and herbicides in agrochemicals, and as powerful cleaning formulations.[86] A major industrial use is in enhanced oil recovery, where they mobilize residual crude oil by achieving ultralow interfacial tension.[87] They also function as nanoreactors for synthesizing uniform nanoparticles. Despite their advantages, challenges include the need for high surfactant concentrations and

potential toxicity of some components. Consequently, contemporary research is directed toward developing eco-friendly, food-grade, and stimulus-responsive microemulsion systems to expand their applicability in green chemistry and targeted delivery.[83]

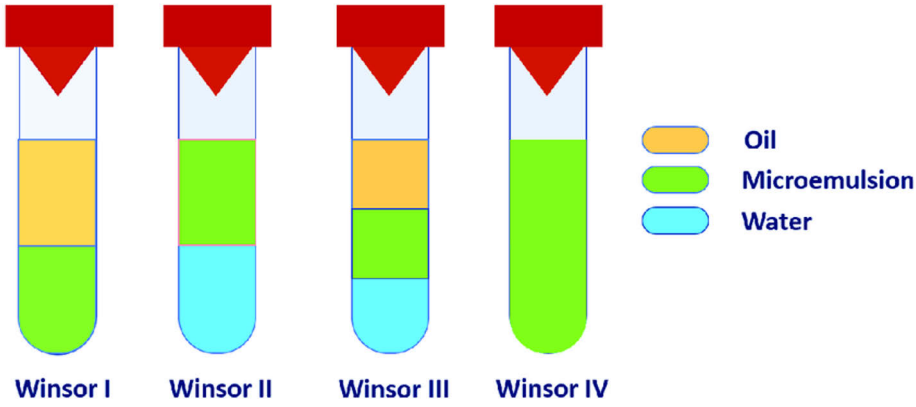

Figure 9. Different types of microemulsion phases reproduced with permission Creative Commons Attribution (CC BY) license[84].

3.3.1 Electrochemistry in microemulsion

Microemulsions represent a more structurally advanced version of conventional biphasic liquid systems. While a classical biphasic system consists of two immiscible phases in macroscopic contact, sharing a single planar interface, a microemulsion achieves the spontaneous and thermodynamically stable co-dispersion of oil and water, stabilised by surfactant molecules at the interface.[88] The result is an enormously enlarged interfacial area, often reaching tens to hundreds of square metres per litre, compared to the essentially negligible interface of a conventional two-phase system. This structural amplification is not merely quantitative: it fundamentally changes the physicochemical environment available for chemical and electrochemical reactions.[89] Reactants that would otherwise be confined to separate phases can now interact where the local polarity, viscosity, and dielectric constant differ markedly from those of either bulk phase.[90] In this sense, microemulsions are not simply "better biphasic systems", they are a distinct class of medium with unique properties.

In principle, any electrochemical or chemical process that has been demonstrated in a biphasic system can be revisited and extended in a microemulsion framework, provided that the additional complexity of the medium is properly accounted for. Processes such as hydrogen evolution at liquid–liquid interfaces[91–93], biphasic redox flow batteries[94,95], electrosynthesis at the oil–water interface[94,95], catalytic reactions

exploiting interfacial partitioning[96,97], and phase-transfer-assisted electrochemical transformations[89] all have direct microemulsion analogues, and in many cases, superior performance in the microemulsion form. The expanded interfacial area accelerates interfacial reaction rates, and the ability to simultaneously solubilise hydrophilic and hydrophobic reactants within the same medium removes the mass-transfer bottlenecks inherent to macroscopic biphasic designs. Furthermore, the composition of microemulsions, the oil-to-water ratio, surfactant type and concentration, and the addition of co-surfactants provides a rich set of tuneable parameters that allow the local reaction environment to be systematically optimised in ways that are simply not possible in a conventional two-phase system.[98]

The introduction of microemulsion structure, however, makes the electrochemistry considerably more complex than in either a simple aqueous medium or a conventional biphasic system.[99] The apparent diffusion coefficient of an electroactive species in such a system is no longer a single, well-defined quantity, because the distribution of molecules between phases is itself dynamic and nonequilibrium in nature.[100] As Balaj et al. demonstrated, nonionic surfactants partition into oil droplets on a timescale of minutes, reaching a nonequilibrium steady-state concentration orders of magnitude higher than in the aqueous phase, before being released back into the water as the droplets solubilise over hours, transiently generating a microemulsion phase at the droplet–water interface. This nonequilibrium partitioning means that an electroactive species does not reside statically in oil, surfactant film, or aqueous pseudophase, but redistributes continuously across all three microenvironments, each with its own local viscosity and dielectric properties, making the measured apparent diffusion coefficient a time-dependent, composition-sensitive composite rather than a fixed material property.[100]

Electron transfer kinetics are similarly governed by the microemulsion architecture rather than bulk solvent properties. In a conventional solvent, when an electron is transferred, the surrounding solvent molecules must physically rearrange themselves to accommodate the new charge distribution on the redox species, a process that costs energy and limits the reaction rate.[101] In a microemulsion, the surfactant layer removes much of this burden by pre-organising the system: it co-localises the oil-soluble electroactive species and the charge-compensating aqueous ions within molecular-scale distances across its hydrophobic tail and hydrophilic head group regions, so that the local environment around the redox centre is already well-suited for charge transfer before the reaction even begins. This structural pre-organisation minimises the solvent reorganisation energy and enables rapid electron transfer rates comparable to those required in high-performance redox flow batteries.[101] What makes this particularly striking is that this fast kinetics is achieved despite the electrode surface being covered by an adsorbed surfactant film, a layer that would intuitively be expected to act as a physical barrier blocking access to the

electrode. Instead, the surfactant film acts as a molecular organiser, bringing reactive species and charge-compensating ions into proximity at the interface and thereby facilitating rather than impeding the electrochemical reaction, a behaviour that is mechanistically reminiscent of membrane-bound enzymes in biological systems.[101]

In other hand, surfactant adsorption at the electrode surface can introduce a further complexity tied directly to the microemulsion structure. Szymula and Narkiewicz-Michałek showed by cyclic voltammetry at a glassy carbon electrode that an organised sodium dodecyl sulfate (SDS) adsorption layer progressively shifts the oxidation peak potential of hydrophobic analytes to more positive values, reflecting the energy barrier imposed by the adsorbed film on charge transfer.[102]

Voltammetric responses in microemulsions exhibit broadened peaks and shifts in apparent formal potentials, reflecting the heterogeneous distribution of redox species across distinct microdomains and their differing local environments.[103]

4 Contextualization and Research Objectives

Research Context

Electrochemical energy storage is a key enabler for the large-scale integration of renewable energy. Among available technologies, redox flow batteries offer distinct advantages due to their scalability and operational flexibility. However, their broader deployment is limited by challenges related to energy density and electrolyte stability.

To overcome these limitations, this thesis explores two complementary research directions. The first focuses on biphasic electrolyte systems, including both liquid–liquid biphasic systems and microemulsions, where structural heterogeneity enables new modes of ion transport and phase behavior. The second direction investigates novel redox chemistries for flow batteries, aiming to introduce a new molecule and improve overall system performance.

Research Objectives

The objectives of this thesis are structured around these two main components:

1. Biphasic and Microemulsion Systems

I. To investigate the utilization of the Galvani potential difference in flow batteries

II. To evaluate how microstructure and water distribution influence conductivity and stability of electrolyte

2. New Chemistry for Flow Batteries

I. To develop and characterize new redox-active species and electrolyte formulations

II. To investigate the capacity recovery

Key Challenges and Novelty

A key challenge in biphasic and microemulsion electrolytes is unlike homogeneous systems, ion transport occurs across heterogeneous aqueous–organic domains and interfaces, where differences in solvation and dielectric properties lead to non-uniform ion distributions and interfacial potential differences. In addition, small compositional changes can affect the system's behavoiur

For new redox chemistries in flow batteries, the main challenge is achieving simultaneous stability, solubility, and electrochemical reversibility while maintaining compatibility with structured electrolyte environments. To place the results of this thesis in a broader context, it is useful to compare the proposed systems with state-of-the-art flow battery technologies.

Practical Considerations

Key performance metrics such as energy density, efficiency, and capacity retention provide a reference for evaluating the potential of biphasic and microemulsion-based electrolytes relative to established aqueous and non-aqueous systems.

Long-term stability remains an important challenge. In structured electrolytes, changes in phase behavior or microstructure over time may affect ion transport and overall performance. Similarly, newly developed redox chemistries may face limitations related to chemical stability, crossover, and reversibility, which can impact operational lifetime.

Finally, practical implementation requires consideration of scalability and industrial relevance. Beyond electrochemical performance, factors such as material cost, system robustness, and compatibility with existing flow battery designs are critical. Addressing these aspects will be essential for translating the concepts developed in this work into viable energy storage technologies.

5 Experimental Techniques

In this chapter, the electrochemical and spectroscopic techniques used to investigate the studied systems are presented. The electrochemical methods include cyclic voltammetry (CV) and flow battery testing, which are used to evaluate the electrochemical behaviour, redox properties, and performance of the systems. While spectroscopic techniques, including nuclear magnetic resonance (NMR) and ultraviolet–visible (UV–Vis) spectroscopy, are described as tools for analyzing molecular structure and composition.

5.1 Electrochemical techniques

5.1.1 Galvanostatic charge and discharge

Battery charge/discharge tests are typically performed using custom-built flow battery cells to assess the practical energy storage performance of the systems. During these experiments, electrolyte solutions containing the redox-active species are pumped through the cell compartments separated by an ion-exchange membrane using solvent-compatible tubing. To evaluate the cell voltage profiles, coulombic voltage and energy efficiencies, and long-term cycling stability measurements can be carried out under constant current (CC) or constant voltage (CV). These tests allowed for direct comparison between different solvent systems and membrane types, revealing how variations in interfacial properties and ionic transport affect the overall battery performance and stability.[104,105]

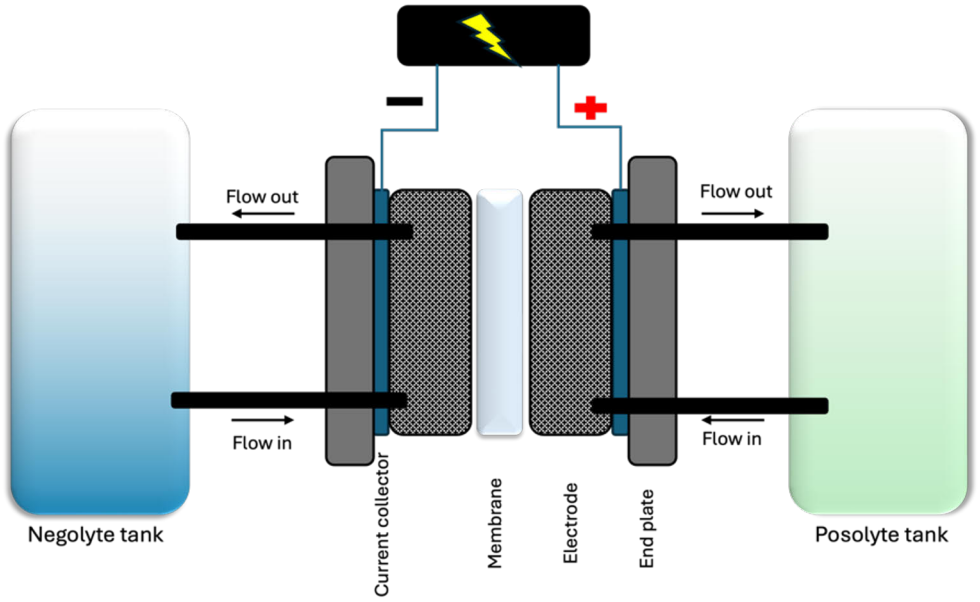

Figure 10. Schematic of a flow battery cell.

Flow battery performance evaluation employs several critical efficiency metrics that quantify different aspects of energy loss and system behavior. Coulombic efficiency (CE), calculated as the ratio of discharge capacity to charge capacity (typically expressed as a percentage), measures the fraction of charge successfully recovered during discharge and reveals losses from parasitic side reactions, active species crossover through the membrane, and self-discharge mechanisms. The coulombic efficiency is expressed as:[106]

$$CE\ (\%) = \frac{Q_{\text{discharge}}}{Q_{\text{charge}}} * 100 \tag{11}$$

where Q represents capacity. Voltage efficiency (VE), defined as the ratio of average discharge voltage to average charge voltage, accounts for overpotentials and internal resistances that cause the battery to discharge at lower voltages than it charges, directly reflecting energy losses due to polarization effects:[106]

$$VE\ (\%) = \frac{V_{\text{discharge,avg}}}{V_{\text{charge,avg}}} * 100 \tag{12}$$

Energy efficiency (EE), the product of coulombic and voltage efficiency, represents the overall round-trip efficiency and determines the economic viability of the system:[107]

$$EE\ (\%) = \frac{E_{\text{out}}}{E_{\text{in}}} * 100 \tag{13}$$

Current density (j), measured in mA/cm² or A/cm², normalizes the operating current by the active electrode area and serves as a key performance indicator:[107]

$$j = \frac{I}{A} \tag{14}$$

where I is the current in amperes and A is the active electrode area in cm². The systems that can perform higher current densities indicate more compact, powerful systems, but if they cannot tolerate it, then it results in increased polarisation losses and can lead to mass transport limitations when electrolyte supply cannot keep pace with electrochemical reaction rates.

Differential capacity analysis (dQ/dV) transforms conventional charge-discharge curves into powerful diagnostic tools by plotting the derivative of capacity with respect to voltage, converting gradual voltage plateaus into sharp, well-defined peaks that correspond to specific electrochemical processes. The differential capacity is calculated as:[108]

$$\frac{\mathrm{d}Q}{\mathrm{d}V} = \frac{\Delta Q}{\Delta V} \tag{15}$$

or in terms of current and potential changes:

$$\frac{\mathrm{d}Q}{\mathrm{d}V} = \frac{I}{\mathrm{d}V/\mathrm{d}t} \tag{16}$$

Each peak in a dQ/dV plot represents a voltage region where capacity changes most rapidly, revealing phase transitions, identifying distinct redox reactions that may overlap in standard voltage profiles, and highlighting degradation mechanisms such as the emergence of new side reactions or the loss of active material. This technique is particularly valuable for detecting subtle changes in battery behavior over cycling, as shifts in peak positions indicate changes in reaction thermodynamics while changes in peak intensity reflect changes in the quantity of active species participating in reactions.

State-of-charge (SOC) is analysed to understand how performance varies across the operating window expressed as:[109]

$$SOC\ (\%) = \frac{Q_{\mathrm{available}}}{Q_{\mathrm{start}}} * 100 \tag{17}$$

where $Q_{\mathrm{available}}$ is the remaining charge that can be extracted and Q_{start} is the available maximum capacity at the beginning of the cycle.

In this thesis, the technique was employed across all **Publications I–III**, as it forms the basis of battery efficiency evaluation. The constant current (CC) method was predominantly used in **Publications I–III** due to its shorter cycle time. This enabled a greater number of cycles in Publications **I–II** and helped minimize dimerization effects in **Publication III**.

5.1.2 Cyclic Voltammetry (CV)

Cyclic Voltammetry is a powerful potentiodynamic electrochemical technique used to study the redox properties and mechanisms of electroactive species. In a typical CV experiment, the working electrode potential is swept linearly with time between two set limits, known as the switching potentials, while the resulting current is measured. The forward scan drives the electrochemical reaction (e.g., oxidation of a species R to O) once the potential is positive enough, and the reverse scan drives the complementary reaction once a sufficiently negative potential is applied (e.g., reduction of O back to R).[110]

The analysis of a cyclic voltammogram provides critical insights into the thermodynamics and kinetics of the electron transfer process. For a reversible, diffusion-controlled redox couple (e.g., ferrocene), the peak current (i_p) is described by the Randles-Ševčík equation:[111]

$$i_p = 2.69 \times 10^5 \, n^{3/2} \, A \, C \sqrt{D\nu} \tag{18}$$

where:
i_p is the peak current (Amperes), n is the number of electrons transferred in the redox event, A is the electroactive area of the working electrode (cm²), D is the diffusion coefficient of electroactive species (cm²/s), C is the bulk concentration of the species (mol/cm³), and ν is the scan rate (V/s).

The linear dependence of the peak current (i_p) on the square root of scan rate ($\nu^{1/2}$) is a hallmark of a diffusion-controlled process. Plotting i_p vs. $\nu^{1/2}$ and observing a linear relationship indicates diffusion-controlled mechanism.
For a reversible system, the separation between the anodic peak potential (E_{pa}) and the cathodic peak potential (E_{pc}) is a key diagnostic criterion:[111]

$$\Delta E_p = E_{pa} - E_{pc} \approx 59/n \text{ mV} \tag{19}$$

This value is approximately 59 mV for a simple, one-electron (n=1), Nernstian (electrochemically reversible) process at 25° C. A larger peak separation indicates slower electron transfer kinetics, signifying a quasi-reversible or irreversible system.

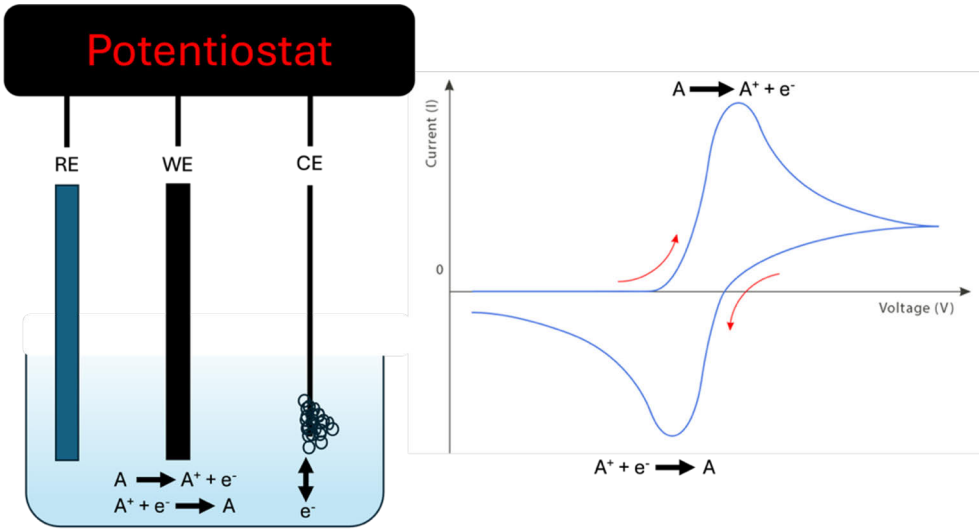

Figure 11. Working principle of cyclic voltammetry.

In this thesis, cyclic voltammetry (CV) was employed across **all Publications I–III** as an initial diagnostic technique to evaluate the electrochemical reversibility of the active species in the electrolyte and to determine their redox potentials. Different reference electrodes were used throughout the studies. In **Publication I**, both organic and aqueous reference electrodes were applied, whereas in **Publications II and III**, only aqueous reference electrodes were used.

5.2 Spectroscopic techniques

5.2.1 Nuclear Magnetic Resonance (NMR) spectroscopy

Nuclear Magnetic Resonance (NMR) spectroscopy is a sophisticated analytical technique that exploits the magnetic properties of atomic nuclei to provide detailed information about molecular structure, dynamics, and chemical environment.[112] When placed in a strong external magnetic field, certain atomic nuclei with non-zero spin (such as ^{1}H, ^{13}C, ^{7}Li, and ^{19}F) align either with or against the field, creating discrete energy levels. The energy difference between these spin states depends on the strength of the applied magnetic field and the gyromagnetic ratio, which is a characteristic property of each type of nucleus. Nuclei can absorb radiofrequency energy at a characteristic resonant frequency known as the Larmor frequency, and this absorption forms the basis of NMR detection.[113] The local magnetic field experienced by each nucleus differs slightly from the applied field due to shielding by surrounding electrons, and this variation gives rise to the chemical shift, measured

in parts per million (ppm) relative to a reference compound such as tetramethylsilane (TMS) for ^{1}H. By measuring these resonance frequencies, which are influenced by the electronic environment surrounding each nucleus, NMR generates spectra that serve as molecular fingerprints. The chemical shift, signal splitting patterns, and signal intensities collectively reveal connectivity, functional groups, and three-dimensional arrangement of atoms within a molecule.[114,115]

NMR spectroscopy is extraordinarily versatile, offering both one-dimensional and multidimensional experiments that can elucidate complex molecular structures, study molecular interactions, and monitor dynamic processes in solution or solid state. Spin-spin coupling between neighbouring nuclei causes signal splitting into multiplets, with the coupling constant (J) measured in Hertz providing information about the number of bonds separating interacting nuclei and their relative orientations. The intensity of NMR signals is proportional to the number of equivalent nuclei contributing to each peak, allowing quantitative analysis of molecular composition. Relaxation processes describe how excited nuclei return to equilibrium after radiofrequency excitation: longitudinal relaxation (T_1) characterizes the recovery of magnetization along the direction of the applied field, while transverse relaxation (T_2) describes the loss of phase coherence in the perpendicular plane, with both parameters providing insights into molecular motion and interactions.[116] In chemistry, NMR is the gold standard for structure determination of organic compounds and for tracking reaction progress in real-time. Advanced techniques such as two-dimensional NMR experiments, including COSY (correlation spectroscopy) for identifying coupled protons, HSQC (heteronuclear single quantum coherence) for direct carbon-hydrogen correlations, and HMBC (heteronuclear multiple bond correlation) for long-range connectivity, enable researchers to map out complete molecular structures.[117,118] The nuclear Overhauser effect (NOE) provides crucial spatial information by detecting nuclei that are close together in three-dimensional space (typically within 5 Ångströms), even if they are not directly bonded, making it invaluable for determining molecular conformations and protein structures. Solid-state NMR extends these capabilities to materials like polymers, catalysts, and battery electrodes where traditional solution NMR is not applicable. Beyond traditional chemistry applications, NMR has proven invaluable in biological research for protein structure determination, in medical diagnostics as the basis for magnetic resonance imaging (MRI), and in materials science for characterizing everything from pharmaceutical formulations to geological samples. Its non-destructive nature and ability to provide quantitative, atomic-level information make NMR one of the most important analytical tools across scientific disciplines.[119]

In this thesis, Nuclear Magnetic Resonance (NMR) spectroscopy was employed in both **Publication II** and **Publication III**. In **Publication II**, ^{7}Li NMR and ^{19}F

NMR were used to determine the location of lithium (Li^+) and TB^- species, i.e. to identify the phase in which they reside. These techniques were also applied to investigate how the distribution of these species changes upon increasing the salt concentration in the microemulsion. The ^7Li chemical shift is sensitive to solvent polarity, solvation strength, and ion pairing, allowing the local environment of Li^+ to be inferred from the direction and magnitude of the shift. In a nonpolar organic solvent, weak solvation and partial association with the counter-anion produces a downfield shift, while strong aqueous solvation shifts the signal upfield. In the microemulsion, spatial separation of Li^+ into the aqueous phase and TB^- into the oil phase minimizes ion pairing at low concentrations. As concentration increases, the growing Galvani potential difference polarizes the interface, driving Li^+ accumulation at the oil–water boundary, disrupting solvation, and progressively shifting the signal downfield with peak broadening further reflecting stronger ion–ion interactions and reduced Li^+ mobility near the polarized interface. Similarly, the ^{19}F shift of TB^- reports on its solvation environment, distinguishing its residence in the aqueous or organic phase.[120]

In **Publication III**, ^{13}C NMR was used to confirm the hypothesized reaction mechanisms and confirm the dimer formation.

5.2.2 Ultraviolet-Visible (UV-Vis) spectroscopy

Ultraviolet-visible spectroscopy is a widely used analytical method that examines how molecules interact with light in the UV and visible range, typically between 200 and 800 nanometer.[121] The technique works by measuring how much light a sample absorbs at different wavelengths. When molecules absorb UV or visible light, their electrons jump from lower energy levels to higher ones, creating distinctive absorption patterns. These patterns depend on the molecule's structure, particularly features like aromatic rings, double bonds, and other groups that readily interact with light. The data appear as a spectrum showing how absorption varies with wavelength, which helps identify compounds and understand their electronic properties.[122]

For flow battery studies, UV-vis spectroscopy is particularly useful because it allows researchers to watch what happens to the active materials during battery operation. As the battery charges and discharges, the molecules change their oxidation state, which shows up as changes in the UV-vis spectrum. This makes it easy to confirm that the expected reactions are taking place. The technique also enables concentration measurements using the Beer-Lambert law:[123]

$$A = \varepsilon bc. \tag{20}$$

where A is absorbance, ε is the extinction coefficient or molar absorptivity (a constant for each substance), b is the sample thickness, and c is concentration. This equation works well for moderate concentrations and provides accurate quantification. Another major advantage is that UV-vis can reveal when unwanted reactions occur, degradation products often have different absorption features that show up as new peaks in the spectrum. Since the measurement does not damage or consume the sample, it's ideal for tracking flow battery electrolytes over time.[124]

The UV–Vis spectroscopy technique was used in **Publication III** to analyse the lithium chloranilate molecule during different stages of battery operation. Significant color changes were observed during the charge and discharge processes, allowing the corresponding spectral changes to be monitored and used to verify the hypothesized reaction mechanisms.

6 Materials and Methods

This chapter describes the experimental techniques used to evaluate new materials for flow battery applications. We employ several complementary analytical methods to thoroughly characterize these candidate materials and assess their suitability for use as battery electrolytes.

Cyclic voltammetry is an electrochemical technique that measures how materials respond to applied electrical potential. This method allows us to determine important properties such as the reversibility of redox reactions, the ease with which electrons transfer, and the diffusion coefficients that describe how charged species move through the electrolyte. These measurements provide fundamental information about the electrochemical behaviour of each material.

In addition to electrochemical testing, we use spectroscopic techniques to analyze the chemical structure and composition of the materials. Nuclear magnetic resonance (NMR) spectroscopy provides detailed information about the molecular structure and the environment of specific atoms within the electrolyte, while ultraviolet-visible (UV-Vis) spectroscopy allows us to study light absorption properties and identify the presence of different chemical species in solution.

Finally, we conduct extended battery cycling tests to evaluate practical performance. These tests measure how well the material functions as an electrolyte during repeated charge and discharge cycles. We monitor the material's stability over time and assess its resistance to chemical degradation that may occur during battery operation. Together, these various techniques provide comprehensive information about both the fundamental properties and the practical performance of candidate materials for flow battery systems.

6.1 Chemicals

In the **publication** (**I***)*, ferrocene (Alfa Aesar) and decamethylferrocene (Sigma-Aldrich) were used as redox-active materials. Lithium chloride (Sigma-Aldrich) and lithium tetrakis(pentafluorophenyl)borate ethyl etherate (LiTB, Boulder Scientific) served as supporting electrolytes. The solvents employed were propylene carbonate and 1,2-dichloroethane (both from Sigma-Aldrich) and trifluorotoluene (Thermo

Scientific). A cation exchange membrane (Nafion 117, Ion Power) was used as the separator in all battery cells. Potassium ferrocyanide was obtained from Sigma-Aldrich.

In **publication** (**II**), the same decamethylferrocene, LiCl, LiTB, TFT, and Nafion 117 were used. Tergitol NP-10 was purchased from Sigma-Aldrich. And LiHCF was synthesised by ourselves.

In the **publication** (**III**), lithium ferrocyanide (LiHCF) and lithium chloranilate (ChALi) were synthesized as reported.[125] The Nafion 212 membrane was obtained from Ion Power. Lithium hydroxide (LiOH, VWR Finland).

6.2 Cyclic voltammetry

Cyclic voltammograms (CVs) in **Publications I, II, III** were recorded at room temperature (approximately 20–22 °C) after purging the solutions with N_2 for 10 minutes. Measurements were carried out using either a SP-240 potentiostat (BioLogic, France) or a PalmSens 4 (PalmSens, the Netherlands). Three electrode experiments employed a glassy carbon working electrode (radius 2 mm) and a platinum counter electrode. The reference electrode was either Ag/Ag^+ (10 mM $AgNO_3$ in acetonitrile) as organic or Ag/AgCl (3 M KCl) as water based.

6.3 Battery cycling

Flow battery measurements in **Publications I, II, III** were carried out using a Battery Cycler G340A (LANHE, China) and a Pump BT600M (Baoding Chuangrui, China), with all experiments performed inside an MBraun glovebox. Thermally activated carbon felts (GFD 4.6 mm, SIGRACELL) were used as electrodes for the battery tests, with a membrane area of 5 cm^2. Solve-Flex tubing (MasterFlex) and cell made of polypropylene, compatible with organic solvents, were used in **publications I, II** and cell made of PVC and Masterflex tubing for water-based electrolytes as shown in Figure 12.

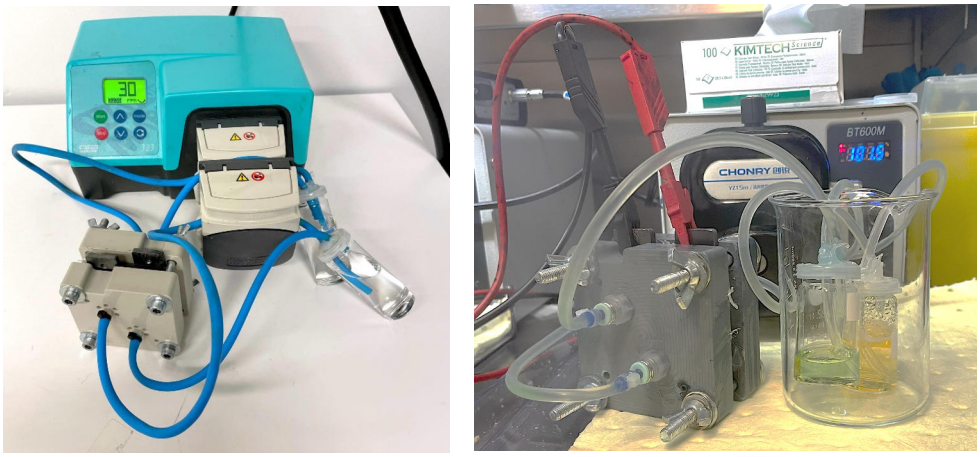

Figure 12. Lab scale flow battery cell used for publication I and II (left) for water-based (right).

6.4 Microemulsion preparation

This formulation constitutes a Winsor IV microemulsion with fluorinated lithium salt to be used as flow battery electrolyte. The system is defined by volume percentages: 42.5% v/v trifluorotoluene (TFT), 42.5% v/v aqueous electrolyte solution, and 15% v/v Tergitol NP-10 surfactant. The aqueous phase is modified with 100 mM LiCl (to total microemulsion volume) to increase ionic conductivity. The PDS is 10 mM LiTB within the total microemulsion volume. LiTB is a highly fluorinated, weakly-coordinating salt that is typically soluble in organic media but can be stabilized in this unique nanoscale environment. The presence of TFT, a fluorinated aromatic polar solvent, provides a compatible organic phase for the LiTB, while the nonionic surfactant Tergitol NP-10 must mediate the interface between this organic phase and the concentrated aqueous electrolyte. The 42.5:42.5:15 volumetric ratio is critical to achieving the thermodynamically stable, and optically clear nanostructured fluid.

A surfactant concentration series is prepared by maintaining a constant 1:1 water-to-oil volume ratio while systematically varying the Tergitol NP-10 content from 1% to 15% (v/v) of the total microemulsion. For each 10 mL sample, the required volumes of trifluorotoluene (TFT) and the aqueous solution are mixed with the addition of LiCl and LiTB at calculated concentrations to yield final global concentrations of 100 mM and 10 mM, respectively. For instance, a sample with 5% surfactant contains 4.75 mL TFT, 4.75 mL aqueous stock, and 0.50 mL NP-10. Each composition is prepared in a sealed 10 mL vial by first combining the TFT and water, followed by dropwise addition of the Tergitol NP-10. Then salts are added to the solution as solids. After complete addition, the vial is vortexed for 2 minutes and then equilibrated in a temperature-controlled bath at 20.0 °C with agitation over

night. Post-equilibration, each sample is assessed for visual clarity and phase number to identify the surfactant percentage range yielding a stable, homogeneous Winsor IV microemulsion.

6.5 *IR* drop measurement

To measure the estimated *IR* drop, during battery electrochemical testing, following the rest period (zero-current condition), applying a current induces an instantaneous potential shift, this potential shift in the first second of the current application reflects the ohmic resistance of the cell, which can be quantified according to Ohm's law. However, it should be noted that the measured current response comprises multiple contributions. While a portion of the current is consumed by faradaic reactions occurring at the electrode surface, the dominant component during the initial transient (within the first second) corresponds to the ohmic resistance of the electrolyte solution. This distinction is important, as the rapid potential jump observed in the early response is primarily governed by the electrolyte conductivity rather than the kinetics of the electrochemical reactions.

7 Biphasic Systems in Flow Batteries

In this chapter, the effect of Galvani potential difference in different systems was investigated showing that flow batteries could take advantages this phenomenon. However, there are some drawbacks including low conductivity and long-term stability for the biphasic systems which are addressed in microemulsion-based electrolytes, as discussed in Chapter 3.3.

7.1 Boosting cell voltage in biphasic flow battery

The biphasic architecture introduces a crucial additional factor: because the two redox couples reside in different chemical environments separated by an immiscible interface, the Galvani potential difference at this liquid-liquid interface can provide an opportunity to enhance the overall voltage output beyond what would be achievable if both couples were in the same phase by focus on ion transfer between phases during battery operation. [60,126]

The authors demonstrate that by carefully selecting solvent combinations with high immiscibility, they can exploit Galvani potential difference to boost the overall cell voltage of the battery. This is essentially free voltage gained purely from the thermodynamic properties of the phase boundary itself, rather than from the intrinsic chemistry of the redox couples. By choosing appropriate solvent pairs, battery designers can potentially add several hundred millivolts to their cell voltage without changing the fundamental redox chemistry, representing a powerful tool for optimizing battery performance.[55]

The degree of immiscibility between solvents (water and oil phase) phase is proportional to the generated Galvani potential difference by partition of salts, greater immiscibility produces more pronounced potential differences.[127] This study investigates polarization at aqueous interfaces with three solvents: trifluorotoluene (TFT), dichloroethane (DCE), and propylene carbonate (PC), with theoretical Galvani potential differences estimated to be 0.805 V, 0.578 V, and approximately 0 V, respectively for Li^+ transfer.

$$E_{\text{cell}} = E_{\text{pos}} - E_{\text{neg}} + \Delta_o^{\text{w}} \phi \tag{21}$$

Table 3. Miscibility organic solvent–water systems.

Organic solvent	Solubility of solvent in water (wt%)	Solubility of water in solvent (wt%)
Trifluorotoluene (TFT)	<0.1	0.04
Dichloroethane (DCE)	0.87	0.16
Propylene carbonate (PC)	17.5	8.30

However, the two immiscible phases must remain separated to ensure stable battery operation. In a flow battery cell, where the electrolytes are continuously circulated, a physical separator is needed that should allow ionic transport, several types of separator materials were investigated. These included high and low EEO (Electroendosmosis) agarose gel, Polytetrafluoroethylene (PTFE) membranes, and polypropylene membranes with both hydrophobic and hydrophilic surface properties. In addition to using these materials individually, different combinations of two separators were also tested to further suppress phase crossover.

Despite these efforts to identify cost-effective alternatives to the expensive Nafion membrane, none of the tested configurations were able to completely prevent mixing of the two electrolyte solutions. Gradual crossover between the phases was observed during operation, eventually leading to mixing in the storage tanks. Depending on the separator configuration, this mixing occurred either within several hours or after a few days of continuous operation. These results indicate that porous membranes and gel-based separators alone were insufficient to fully stabilize the biphasic system under flow conditions. Consequently, a Nafion N-117 membrane was selected due to its well-known cation-exchange properties, chemical stability, and high selectivity for Li^+ ion transport, which helps reducing electrolyte crossover while maintaining ionic conductivity.

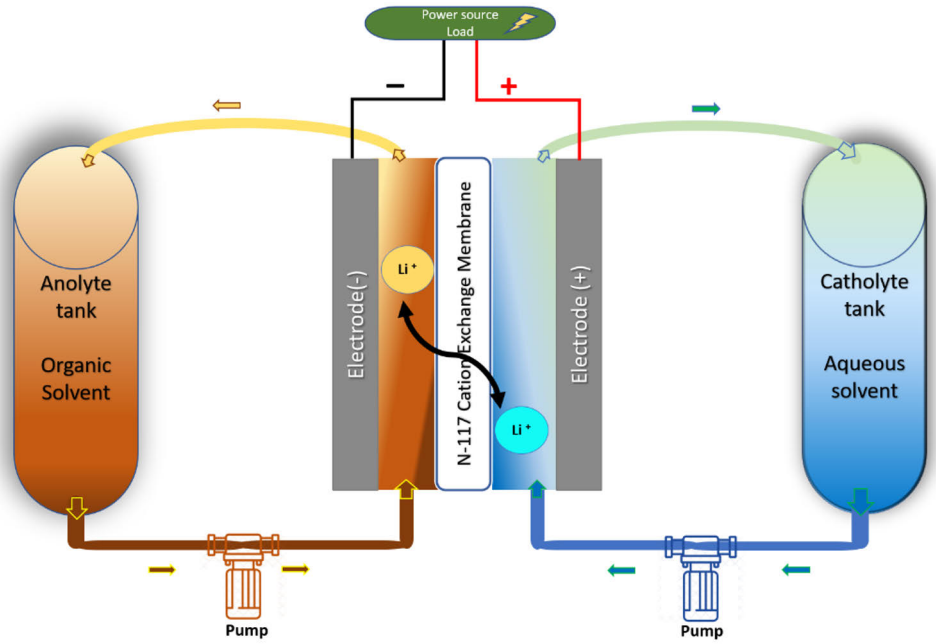

Figure 13. Schematic of a biphasic flow battery indicating the Galvani potential difference of Li^+.

The schematic of the biphasic system is shown in Figure 13. In the posolyte (water phase), 30 mM of both potassium hexacyanoferrate (II) and potassium hexacyanoferrate (III) (referred to as KFCN) in excess, with 100 mM lithium chloride as the supporting electrolyte was chosen as a typical model system. For the organic phase, two typical redox couples Ferrocene (Fc) and Decamethylferrocene (DMFc) in 1-5 mM concentration were utilized along with 10 mM Lithium tetrakis(pentafluorophenyl)borate (LiTB) to polarize the interface. The 10 mM supporting electrolyte in organic phase is sufficient to ensure charge balance and adequate ionic conductivity. The higher concentration of KFCN and higher LiCl are used in posolyte to limit the achieved battery curves and resistances to the organic phase, so the final curves of batteries are from changes in negolyte.
The total equation for the battery during charge is:

Posolyte: $$[Fe(CN)_6]^{4-}(aq) \rightarrow [Fe(CN)_6]^{3-}(aq) + e^- \quad (22)$$

Negolyte: $$Fc^+(o) + e^- \rightarrow Fc(o) \quad (23)$$

Charge equilibrium: $$Li^+(aq) \rightarrow Li^+(o) \quad (24)$$

The total reaction is:

$$[Fe(CN)_6]^{4-}(aq) + Fc^{+}(o) + Li^{+}(aq) \rightarrow [Fe(CN)_6]^{3-}(aq) + Fc(o) + Li^{+}(o) \quad (25)$$

The Gibbs energy change for this reaction can be written as: [62]

$$\Delta G = F(E_{[Fe(CN)6]^{4-}/[Fe(CN)6]^{3-}} - E_{Fc/Fc^{+}}) + \Delta G^{W\rightarrow O}_{tr,Li+} \quad (26)$$

Eq. 26 illustrates that the Gibbs energy of the reaction is composed of the half-cell reactions and the energy to transfer Li^+ from water to oil.[128] With TFT and DCE the standard transfer energy of Li^+ from water to oil is 77.7 kJ/mol or 55.8 kJ/mol, so significantly more energy is required in the charging phase. But upon discharge the same amount of energy is recovered. With PC the transfer energies are close to 0, so the reaction 25 actually becomes spontaneous if Fc is used as the redox couple in PC phase.[129]

The standard transfer energy of Li^+ from the aqueous phase to trifluorotoluene (TFT) is 0.805 V[130], representing the Gibbs free energy change associated with transferring a single lithium ion from water, where it experiences strong solvation due to the high dielectric constant and hydrogen bonding network, to the weakly polar organic phase. This value reflects the intrinsic thermodynamic barrier for desolvating the hydrated ion from its aqueous environment and resolvating it in the organic medium. However, the experimentally observed Galvani potential difference at the water/TFT interface in the presence of LiTB is 0.734 V, representing a 71 mV decrease from the isolated Li^+ transfer energy.[131,132]

This discrepancy arises from the requirement of electroneutrality and the equilibrium partitioning of both ionic species across the interface. The Galvani potential difference is established through the partition equilibrium of the electrolyte salt, not solely by the cation. The TB^- anion exhibits a transfer energy of 0.748 V from water to TFT, indicating its own partitioning preference. At equilibrium, the electrochemical potentials of both ions must be equal in both phases, which can be expressed through the Nernst equation and mass balance considerations. The resulting Galvani potential of 0.734 V represents the equilibrium state where the chemical potential gradients of Li^+ and TB^- are balanced by the electrical potential gradient at the interface. [133,134]

The expected potential of a battery can be calculated based on Eq. 21 when the redox potentials of the active materials and the Galvani potential difference are known. KFCN potential vs. SHE (0.467 V in 100 mM LiCl by Smirnov[135]). The comparison of experimental and theoretical voltages is tabulated in the Table 4.

Table 4. Redox potential of the couple in the organic phase, estimated Galvani potential difference, theoretical cell voltage calculated form Eq. 21 as well as the measured cell voltage.

Oil phase (connected to negative side)	$E^{0'}$ in oil phase vs. SHE (V)	Estimated Galvani potential difference (V)	Theoretical voltage (V)	Measured voltage (V)
DMFc in TFT	0.08	0.734	1.121	0.975
DMFc in DCE	0.07	0.519	0.916	0.852
DMFc in PC	0.055 *	≈ 0	0.412	0.405
Fc in TFT	0.720; or 0.736	0.734	0.481	0.361
Fc in DCE	0.640	0.519	0.346	0.239
Fc in PC	0.576	≈ 0	–0.109	–0.135

*Estimated from cell potential from Fc potential. ** Theoretical voltage means the voltage we expect from Eq. 21, and measured voltage was acquired from experiment at 50% SOC.

Fc and DMFc were tested in the mentioned organic solvents and results are shown in the Figure 14. The measured voltage at ca. 50% state of charge is reported as measured voltage in Table 4. The measured potentials also agree rather well with the expected theoretical values.

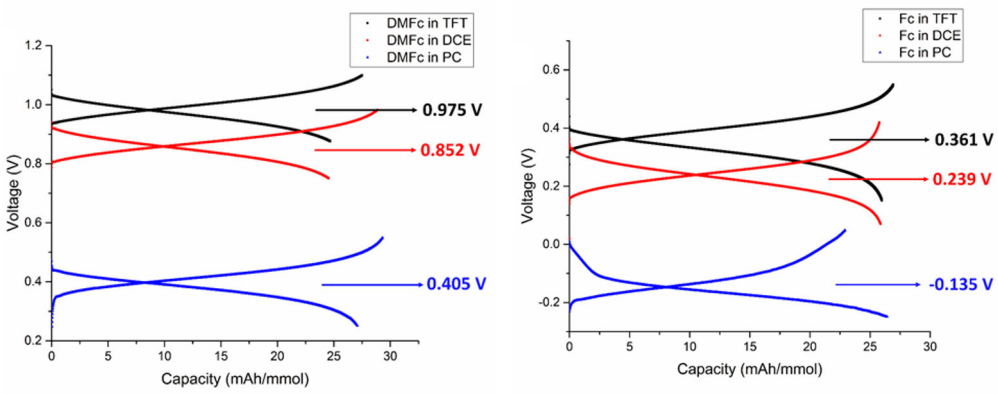

Figure 14. Charge and discharge profiles from battery experiments. Left) Comparing Decamethylferrocene (DMFc) in Trifluorotoluene (TFT), Dichloroethane (DCE), and Propylene Carbonate (PC) Right) Comparing Ferrocene (Fc) in same solvents.

The cell voltages calculated from Eq. 21 exceed the experimentally measured values by approximately 100–150 mV for TFT, 60–100 mV for DCE, and 10–50 mV for PC. This discrepancy may arise from inaccuracies in the method used to determine the standard potential of Fc in PC or KFCN in 100 mM LiCl. Additionally, the observed discrepancy may arise from the membrane potential across Nafion [136] or from non-ideal activity coefficients, particularly in organic solvents. The contribution of activity effects, estimated using the extended Debye–Hückel equation for non-aqueous systems, was approximately −45 mV for TFT, −37 mV for DCE, and negligible for PC, leading to improved agreement between theoretical predictions and experimental voltages. This suggests that the membrane contribution lies in the range of 30–100 mV. Since the standard potentials of DMFc and Fc remain largely unchanged across the different solvents, Figure 14 clearly demonstrates that the cell voltage of biphasic flow batteries can be increased by approximately 600–700 mV through the appropriate selection of solvents and supporting electrolytes. Further enhancement in cell voltage may be achieved by replacing Fc or DMFc with redox couples of more negative potential.

Continuous cycling performance over more than 20 cycles, as demonstrated in Figure 15 confirms the stable operation of biphasic flow batteries under the investigated conditions. Long term cycling degradation is attributed to evaporation of organic solvents.

At the very low current densities employed in this study, no significant polarization losses arise from the ion transfer reaction at the liquid-liquid interface. Higher resistances in the overall system have been attributed to the bulk ionic conductivity of the phases and the membrane separator, rather than interfacial kinetic limitations. The predominant overpotential stems from ohmic resistance rather than activation overpotentials at the phase boundary. Polarization of the interface induced by partitioning of lithium ions between the two phases creates the thermodynamic advantage exploited in these systems. These advantages can be enhanced by minimizing ohmic losses through the selection of high conductivity electrolytes and optimized cell geometries. Alternative strategies include employing low volatility organic solvents to mitigate evaporation or using other ion selective membranes to achieve solution separation without compromising ionic conductivity can be considered to improve the system.

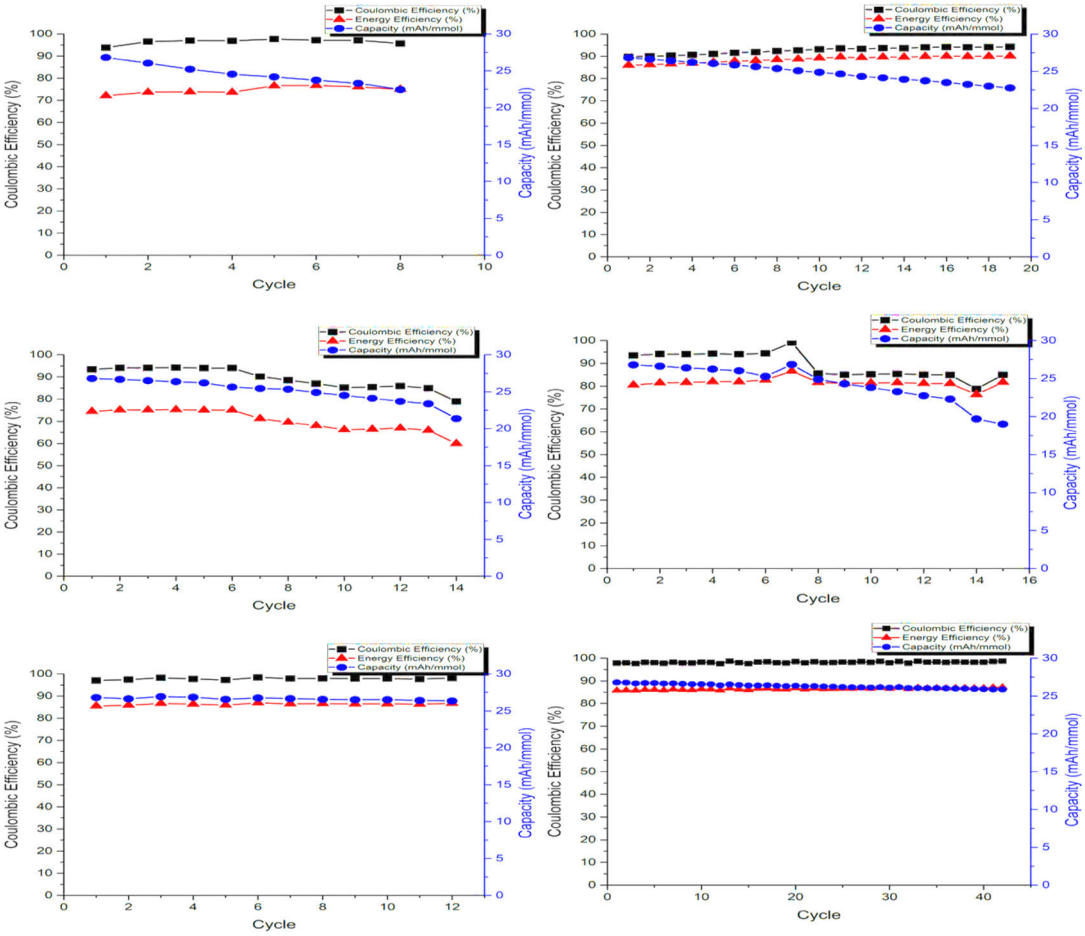

Figure 15. Cycling behaviour of different batteries top-left) Fc in TFT, middle-left) Fc in DCE, and bottom-left) Fc in PC and top-right) DMFc in TFT, middle-right) DMFc in DCE, and bottom right) DMFc in PC, as negolyte vs KFCN in water as posolyte. Current density is 0.2 mA/cm^2.

The implementation of organic solvents in biphasic flow battery systems presents several inherent challenges that must be carefully addressed during system design and operation. The ionic conductivity of organic solvents is substantially lower than that of aqueous electrolytes, typically by several orders of magnitude, which directly impacts the ohmic resistance of the battery and reduces overall energy efficiency. This limitation arises from the lower dielectric constants of most organic solvents compared to water, resulting in reduced ion dissociation and mobility within the organic phase. The volatility of organic solvents poses another significant operational concern, as they exhibit considerably higher vapour pressures than water, leading to increased evaporation rates during battery operation, particularly under

conditions involving elevated temperatures or extended cycling periods. This evaporative loss can alter the composition and volume of the organic phase over time, affecting the concentration of redox active species, changing the ionic strength of the solution and induce precipitation, which can lead to gradual capacity fade. Furthermore, solvent evaporation presents safety and environmental concerns, as many organic solvents are flammable, toxic, or environmentally hazardous. The immiscibility between organic solvents and water, while essential for establishing the Galvani potential difference, creates additional engineering complexities regarding interfacial control, material compatibility with cell components such as current collectors, gaskets, tubing, and membranes, and the prevention of excessive mixing or emulsification that could compromise phase separation. These combined factors necessitate thoughtful system engineering to balance the electrochemical advantages offered by biphasic configurations against the practical challenges introduced by organic solvent utilization.

7.1.1 Membrane at the interface of biphasic flow battery

In the biphasic redox flow battery configuration studied here, a Nafion N-117 cation exchange membrane serves as the ionic separator between two electrolyte tanks. The posolyte is a water-based solution containing LiCl as the supporting electrolyte, while the negolyte consists of an organic solvent containing LiTB as the supporting salt. Nafion N-117 is a well-established perfluorosulfonic acid (PFSA) membrane widely used in electrochemical energy storage applications, including redox flow batteries, owing to its high ionic conductivity, chemical stability, and mechanical durability.[137] To ensure proper conditioning prior to operation, the membrane is pre-soaked in water rather than in the organic solvent. This choice is justified by the substantially faster equilibration kinetics in aqueous media membrane swelling and ion exchange in water occurs within hours, whereas conditioning in organic solvents requires days.[138,139] This difference in uptake kinetics is well documented, and controlling solvent uptake is critical in flow battery applications, as excessive swelling can increase permeability and compromise mechanical integrity. Upon hydration in pure water, the membrane's sulfonate exchange sites become populated by protons (H^+) rather than Li^+, since no lithium salt is present during the pre-soaking step. The membrane therefore enters cell assembly in its proton form, and subsequent ion exchange with Li^+ from the electrolytes occurs in situ once the cell is filled and equilibration begins.

Once assembled, the organic negolyte comes into direct contact with the aqueous-conditioned membrane surface, creating a well-defined water–organic solvent interface at the membrane–negolyte boundary. Because Nafion N-117 functions as a cation exchange membrane, it selectively permits the passage of cations while excluding anions, upon hydration, Nafion phase-separates into an

interconnected network of hydrophilic domains that allow movement of water and cations, but the membrane does not conduct anions. Consequently, the large and hydrophobic TB^- anion present in the organic negolyte is effectively excluded from crossing into the aqueous posolyte. The charge balance across the membrane is therefore governed exclusively by Li^+ transfer. At thermodynamic equilibrium, the partitioning of Li^+ between the organic and aqueous phases, each with different solvation energies and dielectric environments, establishes a Galvani potential difference at the interface. In case the anionic membrane is used, still the membrane is filled with water and the TB^- governs the Galvani potential difference.

7.2 Galvani potential difference in microemulsion-based flow batteries

The goal of this chapter is to extend the advantages of the Galvani potential difference, previously demonstrated in biphasic flow batteries, to microemulsion-based flow batteries. By implementing this concept, an improvement in electrolyte conductivity and cycling stability is expected. In addition, the Galvani potential difference is anticipated to contribute to an increase in the overall battery voltage.

Various compositions of oil, water, and surfactant were tested. The stable monophasic formulation used in this study was 42.5% v/v trifluorotoluene (TFT), 42.5% v/v deionized water and 15% v/v Tergitol NP-10, a non-ionic surfactant (HLB =13.2). LiTB and lithium chloride (LiCl) were added as supporting electrolytes at concentrations of 10 mM and 100 mM, respectively.[140] A redox-active species decamethylferrocene (DMFc), was introduced at a concentration of 1 mM. After all components were combined, the mixture was vortexed for 5 minutes and then allowed to equilibrate at room temperature (25 °C) overnight. The resulting formulation yielded a stable, single phase, and slightly translucent microemulsion shown in Figure 16.

Figure 16. Different microemulsion compositions by different surfactant ratio.

The battery structure is shown in Figure 17. For the battery test, the posolyte is 15 mL aqueous solution containing 10 mM lithium hexacyanoferrate (II) (LiHCF) and 0.5 M LiCl. A 10 mL microemulsion containing 1 mM DMFc as electroactive species is used a negolyte. The negolyte determines that the battery capacity is 268 µAh for 10 µmol of DMFc. Therefore, the charge and discharge curves measured in constant current (CC) mode using a current density of 0.2 mA/cm^2 mainly reflect changes in the negolyte. The charge and discharge cut-off are set at 0.4 V and 0 V, respectively, to prevent side reactions.

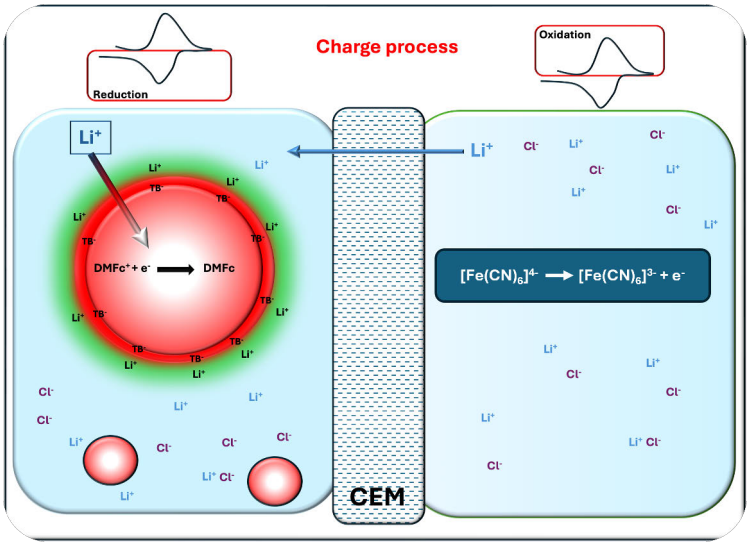

Figure 17. Microemulsion structure used as negolyte and water-based solution as posolyte in the battery.

The $E_{1/2}$ is 0.495 V vs SHE for the posolyte and 0.176 V vs SHE for the negolyte (as depicted in Figure 18. Thus, a battery potential of 0.319 V could be expected. However, 0.195 V is observed in Figure 19 at 50% state of charge (SOC) with 10 mM LiTB in the microemulsion. The 0.124 V decrement is mainly from concentration difference in negolyte and posolyte (0.076 V), also the rest could be from error in measurement of DMFc in microemulsion with Ag/AgCl (3 M KCl) reference electrode, membrane potential over Nafion[136,141], from non-ideal activity coefficient especially in the microemulsion, or forming ionosomes[142] in the oil phase. However, the mentioned effects should affect all the battery results and not just first test, and the first potential drop reason is still not clear to us, it could be from flowing the microemulsion[143–149] and changing viscosity[150–152] or other unknown reasons.

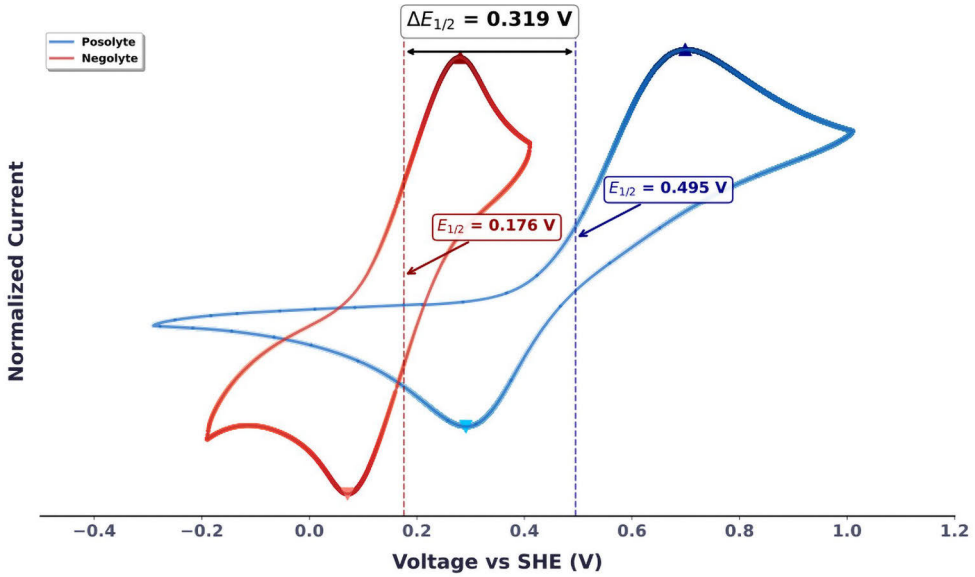

Figure 18. Cyclic voltammograms of the microemulsion used as negolyte (red) and the solution containing LiHCF used as posolyte (blue).

The standard transfer potential of Li^+ ions from TFT solvent to water is 0.805 V[58], and that of TB^- ions is 0.748 V[74], so that their equilibrium distribution should create a Galvani potential difference of 0.777 V when the amount of LiTB is high enough. The initial 10 mM concentration of LiTB in the microemulsion serves primarily to provide ionic conductivity in the oil phase.[140] However, due to the large oil–water interfacial area, this low concentration is insufficient to polarize the interface and induce a measurable Galvani potential difference[120]. To systematically investigate and characterize this electrochemical phenomenon, progressively higher concentrations of LiTB were introduced into the microemulsion system. The experimental protocol involved in-situ addition of LiTB to the microemulsion electrolyte during active battery operation, with incremental concentration increases of 50 mM implemented at each successive stage. This stepwise approach enabled real-time monitoring of the concentration-dependent effects on battery performance while maintaining operational continuity throughout the measurement process. As more polarizing salt is added, the oil–water interface accumulates increasing charge, leading to the development and gradual rise of the Galvani potential difference. At the highest LiTB concentration, the Galvani potential difference reaches its full value 0.777 V. The variation of the Galvani potential difference with the concentration of the polarizing salt is different in microemulsions than the biphasic solutions, because of the large interfacial area of the microemulsions.[153]

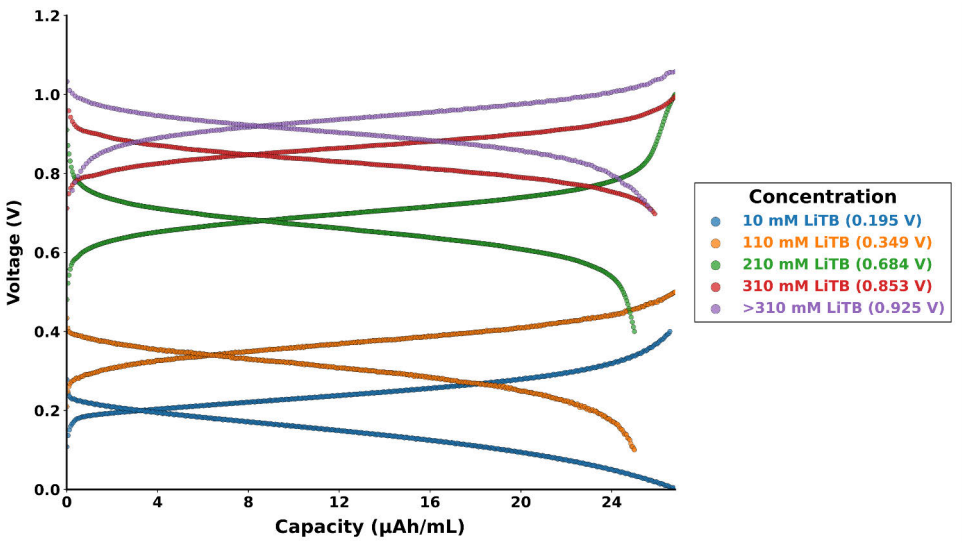

Figure 19. Charge / discharge curves for LiTB concentration steps from 10 mM to over 310 mM. Current density is 0.2 mA/cm$^{2.}$

Figure 19 illustrates the stepwise addition of LiTB to the microemulsion, increasing its concentration from 10 mM to 310 mM in the final step. Afterward, the microemulsion was subjected to evaporation while battery is running, leading to a further increase in LiTB concentration, since the impact of additional salt diminished at higher levels. Thus, the battery can achieve its highest potential simply through increased concentration of LiTB. A detailed overview of the corresponding LiTB concentrations and measured potentials is provided in Table 5.

This improvement in potential also indicates enhanced ionic conductivity within the system. At a LiTB concentration of 10 mM, the internal resistance is relatively high, as reflected by a greater *IR* drop. As the LiTB concentration increases, the resistance decreases. Specifically, the *IR* drop is reduced from 70 mV at 10 mM LiTB to 33 mV in the more concentrated microemulsion as tabulated in Table 5, confirming that higher salt concentrations lead to improved conductivity and more efficient electrochemical performance.

Table 5. Effect of the addition steps varying the LiTB concentration in the microemulsion on the battery potential, the $\Delta\phi$ contribution and the *IR* drop (considering the 1 mA current used). It is assumed that the Galvani potential difference reaches its full value at the evaporation step

Addition step	LiTB / mM	Battery potential / V	$\Delta\phi$ / V	Estimated *IR* / mV
0	10	0.195	0.047	70
1	60	0.307	0.159	60
2	110	0.349	0.201	52
3	160	0.491	0.343	40
4	210	0.684	0.536	35
5	260	0.767	0.619	53
6	310	0.853	0.705	50
evaporation	> 310	0.925	0.777	33

To evaluate potential stability, the battery was cycled at with 210 mM LiTB for 80 cycles, as shown in Figures 20a and 20b, and at 310 mM LiTB for 200 cycles, as shown in Figures 20c and 20d. The battery potential remained stable before and after cycling, indicating that the contribution from the Galvani potential difference is maintained over time also in microemulsions. At 210 mM LiTB concentration the battery demonstrated a coulombic efficiency exceeding 95% and an energy efficiency above 90%, confirming good reversibility. Similarly, at 310 mM LiTB concentration the coulombic efficiency exceeded 97% and energy efficiency remained above 90%, demonstrating that the microemulsion-based battery performs reliably under extended cycling.

The theoretical capacity is 268 μAh but as there was some samplings for NMR analysis which is the main reason capacity is decreasing over this experiment, also the battery charge/discharge is on constant current mode process, it is not possible to reach the full capacity. However, in Figures 20C & D, if the charge cutoff was higher, the capacity would be higher. Capacity fade was limited to 0.25% per cycle after 80 cycles at 0.767 V (210 mM LiTB), and only 0.07% per cycle over 200 cycles at 0.925 V (> 310 mM or 335 mM LiTB). In contrast, the biphasic flow battery using TFT as the solvent exhibited a much higher capacity decay of 0.53% per cycle. These results indicate that the microemulsion system not only enhances conductivity but also improves cyclability compared to biphasic systems.

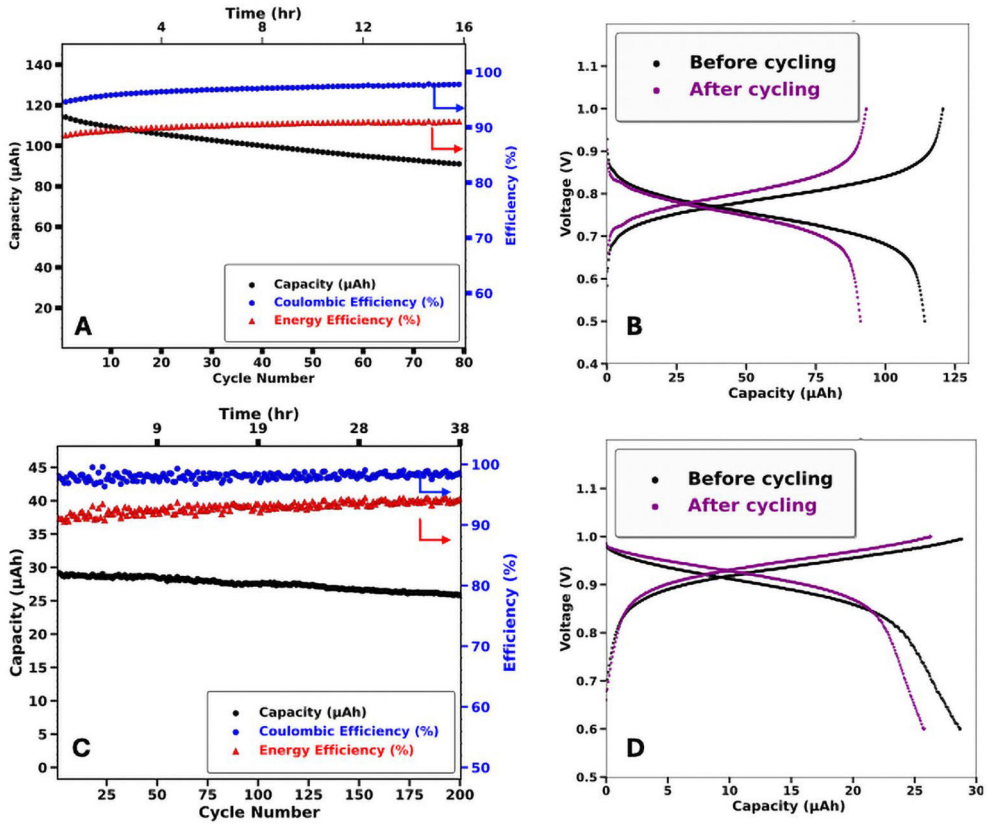

Figure 20. Battery cycle performance: 210 mM LiTB (0.767 V) (A, B) and at > 310 mM or 335 mM LiTB (0.925 V) (C, D). Current density is 0.2 mA/cm^2.

One of the key challenges encountered during testing was the temporal instability of battery potential upon stepwise increases of LiTB concentration in the negolyte. Each addition of LiTB initially produced the expected rise in potential; however, after several hours, the potential began to decline, only to recover again upon the next addition. The root cause was identified as a concentration imbalance across the membrane: the posolyte was initially prepared at 100 mM LiCl, and once the LiTB concentration in the negolyte exceeded this value, Li^+ ions migrated through the Nafion membrane from the negolyte into the posolyte down their concentration gradient, thereby dissipating the Galvani potential difference that had been established. To suppress this cross-membrane equilibration, the posolyte LiCl concentration was raised to 500 mM and maintained at that level throughout subsequent experiments, which effectively stabilized the potential by ensuring that the aqueous Li^+ activity remained more than that in the negolyte at all tested concentrations.

During the study, microemulsion-based formulations were also evaluated as a replacement for the pure aqueous posolyte, with the aim of better matching the solvent environment on both sides of the membrane. However, introducing an organic component into the posolyte added significant complexity to the system: phase transitions occurred during battery operation as the compositions of both electrolytes evolved, making it difficult to maintain a well-defined and reproducible biphasic configuration. It was therefore decided to retain the pure aqueous posolyte to keep the system as simple and controlled as possible.

Despite its advantages, the microemulsion system presents several challenges. One limitation is the use of trifluorotoluene as the oil phase, which requires specialized materials and tubing due to its chemical compatibility issues. Additionally, at higher concentrations of LiTB (above 200 mM), the system tends to become biphasic, indicating limited stability of the microemulsion. This phase separation warrants further investigation and may be mitigated by increasing the surfactant concentration or introducing a co-surfactant to better stabilize the interface. Another observed drawback is the increase in viscosity at higher LiTB concentrations, which can affect mass transport and lead to variations in coulombic and energy efficiencies during cycling.

This work demonstrates that microemulsion-based redox flow batteries significantly benefit from controlled Galvani potential differences across the oil-water interface. By increasing LiTB concentration, the battery exhibited enhanced voltage, lower internal resistance, and improved electrochemical performance. The reduced *IR* drop contributes to more efficient charge-discharge behaviour. Long-term cycling tests confirmed stable performance with high coulombic efficiency and minimal capacity fading over time. Compared to biphasic systems, the microemulsion approach offers improved scalability, reduced membrane requirements, and enhanced mixing, making it a promising platform for next-generation energy storage applications.

8 Investigation of new materials

In this chapter, lithium chloranilate is presented as a novel electrolyte for alkaline negolytes in redox flow batteries. Its properties are investigated through comprehensive characterization, including electrochemical and spectroscopic analyses. Furthermore, battery tests are performed to evaluate its electrochemical performance and applicability in flow battery systems.

8.1 Lithium chloranilate as an electroactive molecule for alkaline negolyte systems

As mentioned, finding cheap and stable organic molecules is one of the primary goals in flow battery research. Quinones[154] have been investigated as an attractive choice for flow batteries due to their natural abundance, low cost, and environmental compatibility. Various types of benzoquinones[155], naphthoquinones[156], and anthraquinones[24,157] are shown in Figure 5.

In **publication III**, a new functionalized quinone molecule is proposed and investigated, as shown in Figure 21 (right). While 2,5-dihydroxy-1,4-benzoquinone has been studied previously, chloranilate offers significant advantages: it is almost ten times cheaper than non-chlorinated derivatives, exhibits high solubility in Li^+ media, and provides a two-electron transfer mechanism.

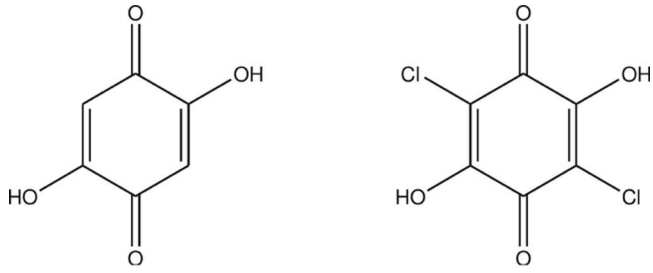

Figure 21. The chemical structures of 2,5-dihydroxy-1,4-benzoquinone (left) and chloranilic acid (right).

In Figure 22 (left), cyclic voltammetry was done in different scan rates from 25–500 mV/s and the results are shown after normalization by the square-root of the scan rate. All the curves are almost overlapping, indicating that the compound has facile kinetics Also, two electrons can be seen in both reduction and oxidation. Based on the cyclic voltammograms, the first electron transfer occurs at –0.78 V and the second at –0.89 V vs Ag/AgCl (3M KCl) in 1M LiOH media. When assembled in a battery with lithium chloranilate as the negolyte and lithium ferrocyanide (LiHCF) as the posolyte, the battery achieves a potential of 1.1 V at the second electron transfer, as depicted in Figure 22 (right).

Different batteries were assembled with varying concentrations of lithium chloranilate (1 mM, 10 mM, and 100 mM), all in 1 M LiOH, paired against an excess of LiHCF posolyte in 1 M LiOH. The batteries were tested under different charge and discharge protocols, and capacity decay was observed. This decay results from dimerization of the charged species, which renders them electrochemically inactive, as shown in Figure 23(left).

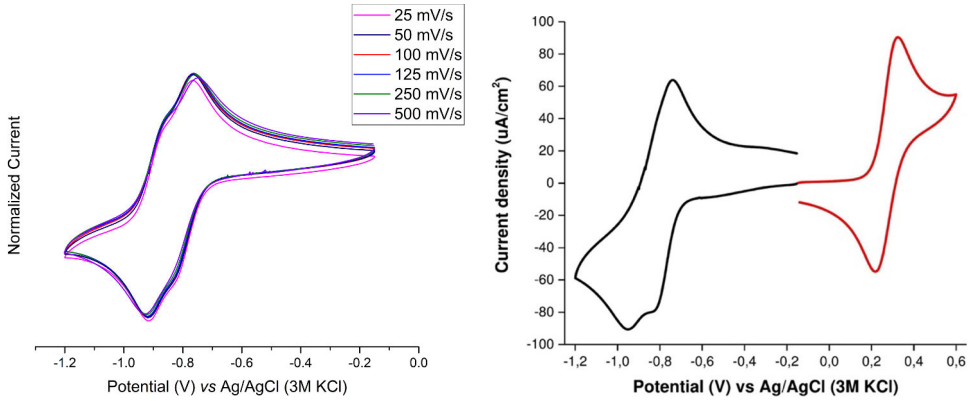

Figure 22. Normalized cyclic voltammetry of 100 mM Lithium chloranilate in 1M LiOH (left) cyclic voltammograms of the lithium chloranilate (black) as negolyte for the battery and lithium ferrocyanide (red) as posolyte side of the system in 1 M LiOH with a 50 mV/s scan rate (right).

The battery performance at 1, 10 , and 100 mM chloranilate concentrations in 1M LiOH is shown in Figure 23. It was observed that higher concentrations of chloranilate resulted in a faster rate of capacity decay. To understand the origin of this behavior, the molecular structure and possible chemical changes of chloranilate during the charge and discharge processes were further investigated.

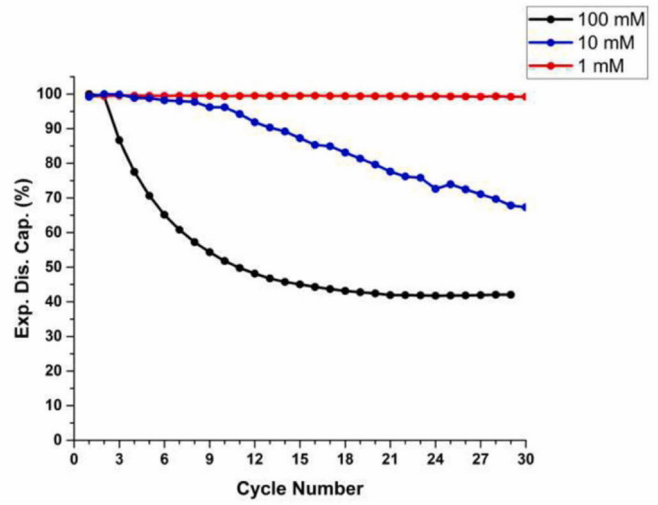

Figure 23. The batteries with different concentration of lithium chloranilate vs LiHCF (Posolyte in excess) in 1 M LiOH.

As a first step, two-negatively charged chloranilate ($C_6Cl_2O_4^{2-}$) can go under one-electron reversible reduction to form a radical species of chloranilate with a charge of –3 as a semi-quinone structure ($C_6Cl_2O_4^{3\bullet-}$). Then it can undergo one-electron reversible reduction to form a chloranilate with charge of –4 as a quinone structure ($C_6Cl_2O_4^{4-}$). The formed chloranilate radical anion species with charge of –3 can irreversibly form a dimeric structure of a quinone ($C_{12}Cl_4O_6^{4-}$) with a charge of –4 in alkaline condition via Eq. 29. During this formation, pH increases as OH^- ions are formed, as evidenced by the color change of green to yellowish.

$$C_6Cl_2O_4^{2-} + e^- \rightarrow C_6Cl_2O_4^{3\bullet-} \quad (27)$$

$$C_6Cl_2O_4^{3\bullet-} + e^- \rightarrow C_6Cl_2O_4^{4-} \quad (28)$$

$$2\ C_6Cl_2O_4^{3\bullet-} + H_2O \rightarrow C_{12}Cl_4O_6^{4-} + 2\ OH^- + 1/2\ O_2 \quad (29)$$

To recover the capacity, the dimer must be oxidized back to monomers, which can be easily accomplished by bubbling air through the solution.[158] Oxygen molecules in the air can both break the dimer bond to reform monomers and discharge the charged molecules, as shown in Figure 24 (right). Air-purging through the solution outside of the glovebox was performed, and a color change from yellow to purple was observed as oxygen (O_2) decomposes the dimer structure to form two negatively charged chloranilate molecules.

The reaction of the oxygen recover step is shown in Eq. 30:

$$C_{12}Cl_4O_6^{4-} + O_2 \rightarrow 2\ C_6Cl_2O_4^{2-} \quad (30)$$

The formation of the dimer can also account for the observed capacity fade, as it produces a new structure with a different electrochemical potential. One way to reconvert the dimer back to the initial monomer is by applying negative potentials during battery discharge.[159] By force discharging the cell and driving the cell potential to more negative values of approximately E = −0.5 V, the dimer is oxidized in a reaction involving hydroxide ions (OH^-), leading to the breaking of the dimer bond. The resulting species is the doubly charged chloranilate anion. This regeneration step is shown in Figure 24 (left).

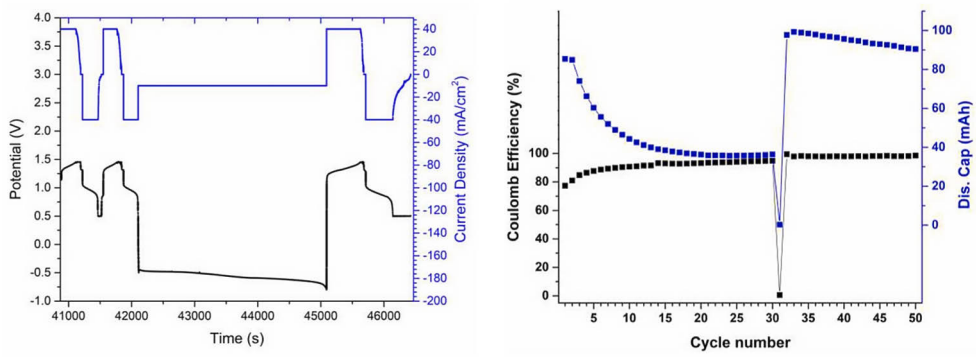

Figure 24. Electro-capacity recovery step (extra-discharging the battery) which breaks the dimer bond (left) The capacity recovery using bubbling air into the solution (right).

The reactions happening in the process is shown in Eq. 31

$$C_{12}Cl_4O_6^{\ 4-} + 4\ OH^- \rightarrow 2\ C_6Cl_2O_4^{\ 2-} + 2H_2O + 4\ e^- \qquad (31)$$

All the reactions and mechanism can be seen from Figure 25.

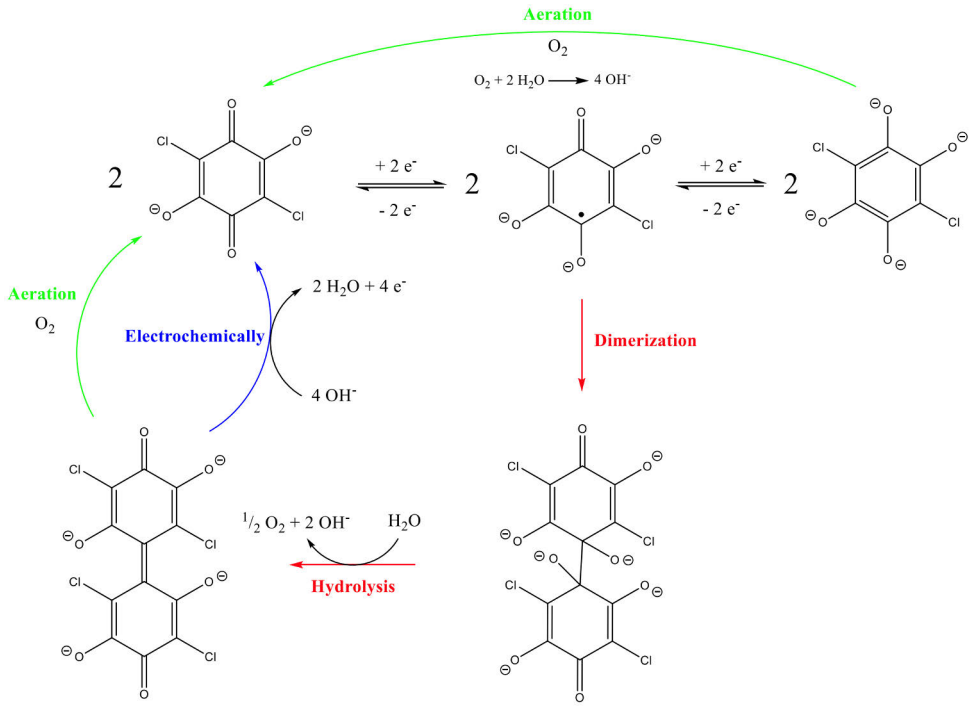

Figure 25. Mechanism of the reaction during charge, discharge and recovery step (both air and electro-).

By performing the electro-recovery step after certain cycles, the battery can last longer, demonstrating the effectiveness of the recovery process. In Figure 26, for a 1 mM negolyte concentration, the recovery step is unnecessary as the dimerization rate at low concentration is negligible. Moreover, applying the recovery step at this concentration not only fails to restore capacity but also depletes active materials, as the high potential can cause destructive oxidation of monomers through side reactions. For the 10 mM and 100 mM concentrations, the decay becomes more pronounced with increasing concentration, requiring more frequent recovery interventions. The recovery protocol was applied after losing 60–70% of the initial capacity. This capacity recovery occurred every 30 cycles for 10 mM and every 10 cycles for 100 mM. The number of cycles between each recovery was kept constant to enable observation of changes following successive recovery steps.

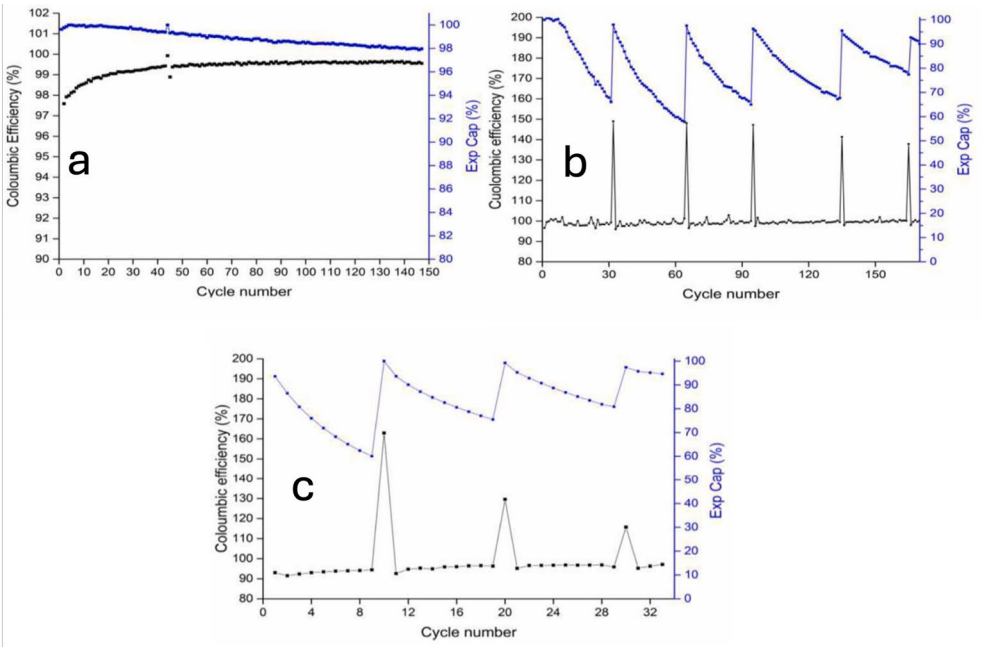

Figure 26. Electro-capacity recovery for different concentration of lithium chloranilate in 1 M LiOH (negolyte); 1 mM (a), 10 mM (b) and 100 mM (c) vs LiHCF (posolyte) in excess.

As the electro-recovery reaction involves 4 OH^-, the solution pH gets lower after each recovery and interestingly the decay rate gets lower. Basically, this implies that the dimerization rate is lower in lower pH. Therefore, the solution was tested in different LiOH concentrations. in figure 27 (left), the black points at the 0.5 M and 0.3 M of LiOH electrolyte are the applied recovery steps which failed because there is no enough OH^- in the media to involve to the recovery step. As a conclusion, there is a trade-off between capacity decay rate and electrolyte concentration. At low concentrations, the decay rate is minimal but capacity recovery is not feasible; at higher electrolyte concentrations, capacity recovery can be successfully implemented to maintain battery operation over extended cycling.

The pourbaix diagram in Figure 27 (right) reveals the potential of the lithium chloranilte is not shifting by changing the pH.

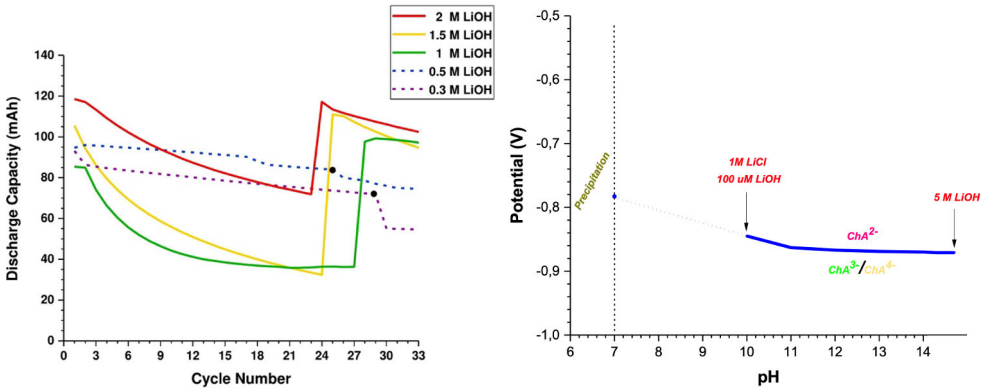

Figure 27. The electrochemical recovery tests for 100 mM LiChA in different LiOH concentrations (left) Pourbaix diagram of chloranilic acid confirms the compound potential stability in different pHs over 10 (right).

The ^{13}C NMR results in Figure 28 show the starting material (left) and the compound after battery cycles in charged state (right). It approves the dimerization forming by addition of peak at 173 ppm.

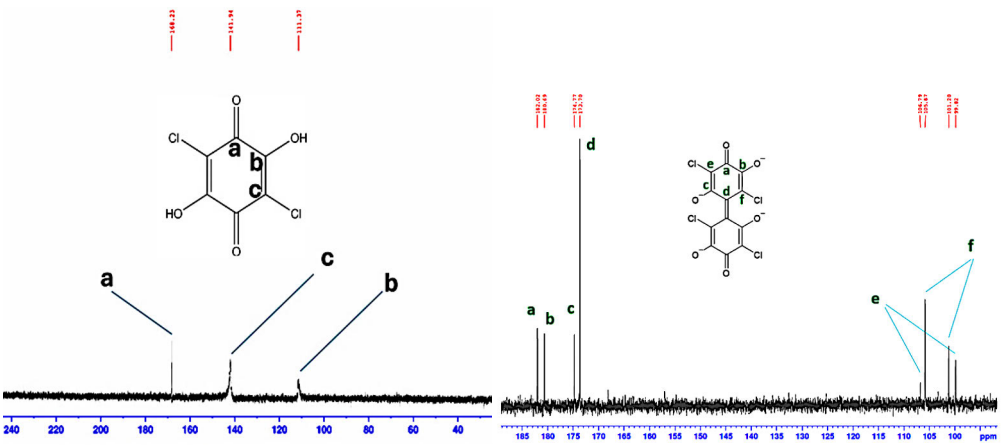

Figure 28. The ^{13}C-NMR spectrum of chloranilate molecule in D_2O (left) The^{13}C-NMR spectrum of formed dimer molecule from hydrolysis of $2e^-$-reduced chloranilate molecule in D_2O (right).

As the negolyte solution has different colors different charge states, the UV-vis test can be employed to approve the mechanism. In Figure 29, UV-vis spectra approve the reaction mechanism and electrorecovery step in the battery by the green line matching the black line showing after recovery step, the dimer is broken into monomers.

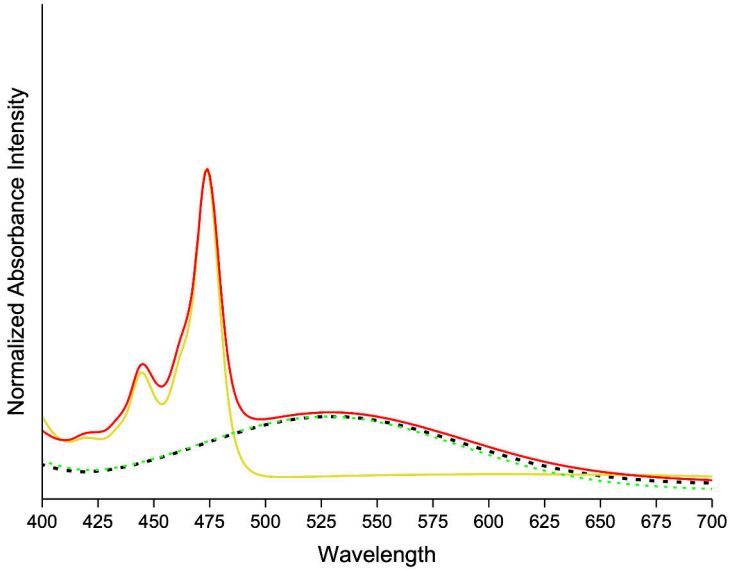

Figure 29. Normalized UV-vis spectra of chloranilate and dimer species before and after electrorecovery (black = starting material, discharged state; red = after overnight charging-discharging at discharged state; yellow = charged state; green = after electrorecovery).

As conclusion, lithium chloranilate represents a cost-effective candidate for use as negative electroactive material in flow batteries. Electrochemical characterization revealed that capacity degradation resulted from dimerization of the chloranilate molecule, which could be reversed through oxidative treatment. Initial studies employed molecular oxygen for this purpose; however, electrochemical oxidation proved more effective at regenerating the dianionic form and restoring capacity. Investigation of operating parameters demonstrated that pH and concentration significantly influence capacity loss during cycling. Higher pH values enhanced compound efficiency and improved achievable capacity. The system demonstrated sufficient reversibility and cycle stability to warrant further development as a viable flow battery chemistry.

9 Conclusion and Outlook

The dissertation focuses on the development of flow batteries chemistry, examining innovative electrochemical systems designed to address the growing demand for large-scale energy storage solutions. This research investigates novel electrolyte formulations and molecular candidates that can enhance the performance and economic viability of flow battery technologies. By exploring alternative redox-active species and biphasic solvent systems, the study aims to overcome the limitations of conventional vanadium-based electrolytes that currently dominate the commercial market. The goal is to advance the field toward more sustainable, cost-effective, and scalable energy storage systems that can support the global transition to renewable energy sources.

The first part contains investigation of using organic solvents in flow batteries by making biphasic and microemulsion-based flow batteries. In **publication I** Different solvents such as trifluorotoluene, 1,2-dichloroethane, and propylene carbonate were tested in the biphasic system. As expected, trifluorotoluene and 1,2-dichloroethane solvents after polarizing the interface with PDS in biphasic flow battery configuration (*vs* water-based) could generate Galvani potential difference for 0.734 and 0.519 V. As the propylene carbonate solvent has polarity and it is a bit miscible in water, so the Galvani potential difference generation was not expected, and the cell voltage was not increased. This study could easily show by engineering the use of organic solvents, it is possible to make higher energy density out of the system with the same volume materials. The drawbacks of this system are low conductivity and low vapour pressure of the solvents used which make it difficult for long-term operation or industry applications. Therefore, in **publication II** microemulsion-based flow batteries are introduced to overcome the mentioned drawbacks. This system uses the trifluorotoluene as it could generate highest Galvani potential difference among the mentioned solvents in previous work. Microemulsion made of water, trifluorotoluene and Tergitol NP-10 (surfactant) was employed as negolyte in the battery and by addition of more PDS the potential is boosted until the maximum Galvani potential difference of 0.777V is reached. The reason for gradual increase of the Galvani potential difference is that the interface in microemulsions is very large compared to biphasic system and it needs more PDS to polarize the

interface. Also, not all the PDS goes at the interface, but it makes ionosomes that does not let them contribute to the interface polarization. The system was cycled in different voltages for days (1000 cycles in total) while the conductivity was improved by a factor of three over the biphasic system.

In the second part, lithium chloranilate molecule was designed to be used in flow batteries. In **publication III**, lithium chloranilate molecule behaviour was investigated in alkaline media as negolyte with two reduction steps at –0.78 V and –0.89 V vs Ag/AgCl (3M KCl). Lithium chloranilate shows promise as a negative electrode material for redox flow batteries due to its low cost. Capacity fades during cycling because the chloranilate molecules dimerize, though this can be reversed with oxidative treatment. Electrochemical oxidation works better than molecular oxygen for regenerating capacity. pH and concentration substantially affect performance, with higher pH improving efficiency and capacity retention. The material exhibits adequate reversibility and stability for further development.

Future work must address the limitations of current microemulsion systems. Formulating with greener organic solvents and lower-cost salts instead of LiTB would improve both sustainability and scalability. However, industrial adoption remains constrained by the poor solubility of electroactive compounds in the organic phase. To enhance solubility, the molecular design of electroactive species, for example, through r alkyl side-chain functionalization, could improve organic-phase compatibility. Alternatively, optimizing the microemulsion composition by introducing co-surfactants or selecting solvents with higher solvation capacity may increase solute loading. Furthermore, using non-ionic surfactants makes these systems sensitive to temperature, necessitating studies to identify an optimal thermal operating window in flow battery configurations. Finally, the effects of pumping on viscosity and phase stability, a rarely studied aspect in flow cells, should be systematically evaluated to assess practical viability.

Acknowledgements

Once I was a master's degree student, I heard and read that a PhD is a long journey and not always a good journey. However, I have usually been a lucky person in my life, so I wanted to try. I think I consumed a big share of my whole luck to get nice supervisors in this chaotic world. Pekka, Ulriika, and Eduardo always cared, supported, and helped me with my stupid questions. Thanks to all of them.

With nice supervisors, a PhD is only 8 out of 24 hr, and for the rest of the time, real friends and family took another big share of the luck. Once you arrive in a new place, the first people who help you are gold. I met my friends Arman and Behzad first and had a good time with them. During the journey, I got married to min fru Maryam, and life became easier and more colourful. Then we got familiar with Taru ja Martti. I think they took the rest of the luck. Really parent-like friends, if you don't know them, then you can't understand. I don't want to forget my best friend, Raji, from Barareh. Also, Hopi, Mohandes, Majid the hirviö, Weronika, and Masoud.

From colleagues, I want to thank Ali, the hard-working lab body who doesn't care about weekends or weekdays. Chanezilla-on-kissa for being nice and always ready to help. I can also mention Eduardo here, as he was my colleague first :D. Patient, available, professional, and hullu. Mahdi-s (both old and new), nice and kind personality. Nichu as the first Chinese I met and Mousumi, nice people. Thank you all for being nice colleagues.

We moved to Aalto for a long-time visit. Great chance to meet new, nice colleagues: Ayesha, Abdullah (Negolye), and Li (second Chinese).

People usually thank the grant sources, but I think we should thank Pekka for writing successful proposals.

I will write my nephews and nieces here, then when they grow up, they won't complain: Kimia, Ilia, Sophia, and Liana.

Finally, I thank my family in Iran: my mom, dad, brothers, and their wives.

Vahid Abbasi
Turku, March 2026

List of References

1. Kandhasamy, M., Duvaragan, B. K., Kamaraj, S. & Shanmugam, G. An Overview on Classification of Energy Storage Systems. in *ACS Symposium Series* vol. 1484 1–25 (American Chemical Society, 2024).
2. Chatzigeorgiou, N. G., Theocharides, S., Makrides, G. & Georghiou, G. E. A review on battery energy storage systems: Applications, developments, and research trends of hybrid installations in the end-user sector. *J. Energy Storage* **86**, 111192 (2024).
3. Zhang, C., Wei, Y. L., Cao, P. F. & Lin, M. C. Energy storage system: Current studies on batteries and power condition system. *Renewable and Sustainable Energy Reviews* **82**, 3091–3106 (2018).
4. Dieterle, M. *et al.* Life cycle assessment (LCA) for flow batteries: A review of methodological decisions. *Sustainable Energy Technologies and Assessments* **53**, 102457 (2022).
5. Duan, W. *et al.* Towards an all-vanadium redox flow battery with higher theoretical volumetric capacities by utilizing the VO2+/V3+ couple. *Journal of Energy Chemistry* **27**, 1381–1385 (2018).
6. Parasuraman, A., Lim, T. M., Menictas, C. & Skyllas-Kazacos, M. Review of material research and development for vanadium redox flow battery applications. *Electrochim. Acta* **101**, 27–40 (2013).
7. Pokhriyal, A., Rueda-García, D. & Gómez-Romero, P. To flow or not to flow. A perspective on large-scale stationary electrochemical energy storage. *Sustain. Energy Fuels* **7**, 5473–5482 (2023).
8. Alotto, P., Guarnieri, M. & Moro, F. Redox flow batteries for the storage of renewable energy: A review. *Renewable and Sustainable Energy Reviews* **29**, 325–335 (2014).
9. Noack, J., Roznyatovskaya, N., Herr, T. & Fischer, P. Die Chemie der Redox-Flow-Batterien. *Angewandte Chemie* **127**, 9912–9947 (2015).
10. Winsberg, J., Hagemann, T., Janoschka, T., Hager, M. D. & Schubert, U. S. Redox-Flow-Batterien: von metallbasierten zu organischen Aktivmaterialien. *Angewandte Chemie* **129**, 702–729 (2017).
11. Soloveichik, G. L. Flow Batteries: Current Status and Trends. *Chem. Rev.* **115**, 11533–11558 (2015).
12. Gandomi, Y. A. *et al.* Critical Review—Experimental Diagnostics and Material Characterization Techniques Used on Redox Flow Batteries. *J. Electrochem. Soc.* **165**, A970–A1010 (2018).
13. Suresh, S. *et al.* Zinc-bromine hybrid flow battery: Effect of zinc utilization and performance characteristics. *RSC Adv.* **4**, 37947–37953 (2014).
14. Shanmugam, S. *et al.* Progress and challenges in zinc-bromine batteries (ZBBs): A path towards safety and mitigation of high-performance systems. *Appl. Energy* **404**, (2026).
15. Wang, W. *et al.* Recent progress in redox flow battery research and development. *Adv. Funct. Mater.* **23**, 970–986 (2013).
16. Waters, S. E., Robb, B. H., Marshak, M. P. & Marshak, M. P. Effect of Chelation on Iron-Chromium Redox Flow Batteries. *ACS Energy Lett.* **5**, 1758–1762 (2020).
17. Sun, C. & Zhang, H. Review of the Development of First-Generation Redox Flow Batteries: Iron-Chromium System. *ChemSusChem* **15**, e202101798 (2022).

18. Colli, A. N., Peljo, P. & Girault, H. H. High energy density MnO4-/MnO42- redox couple for alkaline redox flow batteries. *Chemical Communications* **52**, 14039–14042 (2016).
19. Yang, Z. *et al.* Alkaline Benzoquinone Aqueous Flow Battery for Large-Scale Storage of Electrical Energy. *Adv. Energy Mater.* **8**, (2018).
20. Amini, K. *et al.* An Extremely Stable, Highly Soluble Monosubstituted Anthraquinone for Aqueous Redox Flow Batteries. *Adv. Funct. Mater.* **33**, (2023).
21. Hu, B. *et al.* Improved radical stability of viologen anolytes in aqueous organic redox flow batteries. *Chemical Communications* **54**, 6871–6874 (2018).
22. Nolte, O., Rohland, P., Ueberschaar, N., Hager, M. D. & Schubert, U. S. Stability of TMA-TEMPO-based aqueous electrolytes for redox-flow batteries. *J. Power Sources* **525**, (2022).
23. Cui, Y. *et al.* A multi-substituted phenazine derivative aqueous redox flow battery with high energy efficiency and long lifetime. *J. Power Sources* **633**, 236461 (2025).
24. Hu, B., Luo, J., Hu, M., Yuan, B. & Liu, T. L. A pH-Neutral, Metal-Free Aqueous Organic Redox Flow Battery Employing an Ammonium Anthraquinone Anolyte. *Angewandte Chemie* **131**, 16782–16789 (2019).
25. Yang, B. *et al.* A Durable, Inexpensive and Scalable Redox Flow Battery Based on Iron Sulfate and Anthraquinone Disulfonic Acid. *J. Electrochem. Soc.* **167**, 060520 (2020).
26. Gui, S. *et al.* Iron complex with multiple negative charges ligand for ultrahigh stability and high energy density alkaline all-iron flow battery. *J. Power Sources* **628**, 235947 (2025).
27. Pagot, G. *et al.* A green solution to improve the performance of zinc-polyiodide flow batteries. *J. Power Sources* **662**, 238794 (2026).
28. Ma, T., Huang, Z., Xie, X. & Li, B. Evaluation of the effect of hydrogen evolution reaction on the performance of all-vanadium redox flow batteries. *Electrochim. Acta* **504**, 144895 (2024).
29. Pedraza, E. *et al.* Unprecedented Aqueous Solubility of TEMPO and its Application as High Capacity Catholyte for Aqueous Organic Redox Flow Batteries. *Adv. Energy Mater.* **13**, 2301929 (2023).
30. Pan, M. *et al.* Highly soluble and crossover-free all-organic redox pair using N-heterocycle-linked TEMPO and two-electron-capable bipyridinium towards high performance aqueous flow batteries. *Chemical Engineering Journal* **496**, 153504 (2024).
31. Li, X. *et al.* Symmetry-breaking design of an organic iron complex catholyte for a long cyclability aqueous organic redox flow battery. *Nat. Energy* **6**, 873–881 (2021).
32. Yang, K. *et al.* Assembling-induced redox property adjustment of Fe(III)/Fe(IV) electroredox couple-based commercial dye catholyte via bio-inspired multicoordination sphere construction strategy for stable aqueous redox flow batteries. *Energy Storage Mater.* **71**, 103648 (2024).
33. Yang, G. *et al.* An Aqueous All-Quinone-Based Redox Flow Battery Employing Neutral Electrolyte. *Adv. Energy Mater.* **14**, 2400022 (2024).
34. Kim, J. Y. *et al.* Unveiling dominant impact of electrochemical stability on performance deterioration in alkaline redox flow batteries utilizing different benzoquinone derivatives. *J. Power Sources* **611**, 234766 (2024).
35. Sullivan, P. T. *et al.* Viologen Hydrothermal Synthesis and Structure–Property Relationships for Redox Flow Battery Optimization. *Adv. Energy Mater.* **13**, 2203919 (2023).
36. Yao, Y. *et al.* Nonionic oligo(ethylene glycol)-substituted viologen negolytes for aqueous organic redox flow batteries. *J. Mater. Chem. A Mater.* **11**, 12984–12991 (2023).
37. Hu, B., Li, H., Fan, H. & Song, J. A long-lifetime aqueous organic redox flow battery utilizing multi-redox anolyte. *Energy Storage Mater.* **59**, 102789 (2023).
38. Liu, X. *et al.* Arylene Diimide Derivatives as Anolyte Materials with Two-Electron Storage for Ultrastable Neutral Aqueous Organic Redox Flow Batteries. *CCS Chemistry* **5**, 2334–2347 (2023).
39. Ding, Y., Zhang, C., Zhang, L., Zhou, Y. & Yu, G. Molecular engineering of organic electroactive materials for redox flow batteries. *Chem. Soc. Rev.* **47**, 69–103 (2018).

40. Gong, K., Fang, Q., Gu, S., Li, S. F. Y. & Yan, Y. Nonaqueous redox-flow batteries: Organic solvents, supporting electrolytes, and redox pairs. *Energy Environ. Sci.* **8**, 3515–3530 (2015).
41. Huang, J. *et al.* Liquid Catholyte Molecules for Non-aqueous Redox Flow Batteries. *Adv. Energy Mater.* **5**, 1401782 (2015).
42. Winsberg, J., Hagemann, T., Janoschka, T., Hager, M. D. & Schubert, U. S. Redox-Flow-Batterien: von metallbasierten zu organischen Aktivmaterialien. *Angewandte Chemie* **129**, 702–729 (2017).
43. Liu, Q. *et al.* Non-aqueous chromium acetylacetonate electrolyte for redox flow batteries. *Electrochem. commun.* **12**, 1634–1637 (2010).
44. Duan, W. *et al.* A symmetric organic-based nonaqueous redox flow battery and its state of charge diagnostics by FTIR. *J. Mater. Chem. A Mater.* **4**, 5448–5456 (2016).
45. Wei, X. *et al.* Radical Compatibility with Nonaqueous Electrolytes and Its Impact on an All-Organic Redox Flow Battery. *Angewandte Chemie* **127**, 8808–8811 (2015).
46. Wei, X. *et al.* Towards high-performance nonaqueous redox flow electrolyte via ionic modification of active species. *Adv. Energy Mater.* **5**, 1400678 (2015).
47. Noack, J., Roznyatovskaya, N., Herr, T. & Fischer, P. The Chemistry of Redox-FlowBatteries. *Angewandte Chemie* **127**, 9912–9947 (2015).
48. Arevalo-Cid, P., Dias, P., Mendes, A. & Azevedo, J. Redox flow batteries: A new frontier on energy storage. *Sustain. Energy Fuels* **5**, 5366–5419 (2021).
49. Ejigu, A., Elgendy, A., Al Nasser, H. A., Jupp, K. & Dryfe, R. A. W. Membraneless biphasic redox flow batteries: Interfacial effects and generalisation of the chemistry. *Electrochim. Acta* **512**, 145426 (2025).
50. Navalpotro, P. *et al.* Pioneering Use of Ionic Liquid-Based Aqueous Biphasic Systems as Membrane-Free Batteries. *Advanced Science* **5**, 1800576 (2018).
51. Li, X., Qin, Z., Deng, Y., Wu, Z. & Hu, W. Development and Challenges of Biphasic Membrane-Less Redox Batteries. *Advanced Science* **9**, 2105468 (2022).
52. Abbasi, V. & Peljo, P. Boosting the cell voltage in biphasic flow batteries via Galvani potential difference. *Physical Chemistry Chemical Physics* **26**, 17476–17480 (2024).
53. Tomazic, G. & Skyllas-Kazacos, M. Redox Flow Batteries. in *Electrochemical Energy Storage for Renewable Sources and Grid Balancing* 309–336 (Elsevier Inc., 2015).
54. Mareček, V. & Samec, Z. Ion transfer kinetics at the interface between two immiscible electrolyte solutions supported on a thick-wall micro-capillary. A mini review. *Current Opinion in Electrochemistry* **1** 133–139 (2017).
55. Peljo, P., Bichon, M. & Girault, H. H. Ion transfer battery: Storing energy by transferring ions across liquid-liquid interfaces. *Chemical Communications* **52**, 9761–9764 (2016).
56. Gavach, C., Seta, P. & Henry, F. A Study of the Ionic Transfer across an Aqueous Solution \ &iquid Membrkmi Interface by Chronopotentiometric and Impedance Measurements *. *Bioelechochemistry and Bioenergefics* **1**, 329–342 (1974).
57. C. Gavach. Kinetics of Electroadsorption and Polarization at the Interface Between Certain Nonmiscible Ionic Solutions. *Experientia Suppl.* **18**, 321–331 (1971).
58. Liu, J. *et al.* Electrochemical Study of Ion Transfers Processes at the Interfaces between Water and Trifluorotoluene and Its Derivatives. *ChemElectroChem* **9**, e202200389 (2022).
59. Reymond, F., Steyaert, G., Carrupt, P.-A., Testa, B. & Girault, H. Ionic Partition Diagrams: A Potential-pH Representation. *J. Am. Chem. Soc.* **118**, 11951–11957 (1996).
60. Alexander G. Volkov, D. W. D. *Liquid-Liquid InterfacesTheory and Methods*. (Boca Raton, 1996).
61. Peljo, P. & Girault, H. H. Liquid/Liquid Interfaces, Electrochemistry atUpdate based on the original article by Frédéric Reymond, Hubert H. Girault. in *Encyclopedia of Analytical Chemistry* (Wiley, 2012).

62. Eugster, N., Fermín, D. J. & Girault, H. H. Photoinduced electron transfer at liquid/liquid interfaces. Part VI. On the thermodynamic driving force dependence of the phenomenological electron-transfer rate constant. *Journal of Physical Chemistry B* **106**, 3428–3433 (2002).
63. Hundhammer, B., Miiller, C., Solomon, T., Alemu, H. & Hassen, H. Ion transfer across the water-o-dichlorobenzene interface. *J. Electroanal. Chem* **319**, 125–135 (1991).
64. Killeen, C., Kropp, A., Chagunda, I., Jackson, E. & McIndoe, J. S. The amenability of different solvents to electrospray ionization mass spectrometry. *International Journal of Mass Spectrometry* Preprint at (2024).
65. Sherwood, J. European Restrictions on 1,2-Dichloroethane: C-H Activation Research and Development Should Be Liberated and not Limited. *Angewandte Chemie* **130**, 14482–14486 (2018).
66. Barthel, J., Neueder, R. & Roch, H. Density, relative permittivity, and viscosity of propylene carbonate+dimethoxyethane mixtures from 25 °C to 125 °C. *J. Chem. Eng. Data* **45**, 1007–1011 (2000).
67. Wolfgang Schmickler & Elizabeth Santos. 18. Liquid-liquid interfaces. in *Interfacial Electrochemistry* 217–234 (Springer Nature, 2010).
68. A.J. Olaya, P. G. H. H. G. Ion transfer across the water|trifluorotoluene interface. *Electrochem. commun.* **19**, 101–104 (2012).
69. Vanýsek, P. & Ramírez, L. B. INTERFACE BETWEEN TWO IMMISCIBLE LIQUID ELECTROLYTES: A REVIEW. *J. Chil. Chem. Soc* **53**, 1455–1463 (2008).
70. Girault, H. H. *Analytical and Physical Electrochemistry*. (EPFL Press, 2004).
71. Trojánek, A., Mareček, V., Langmaier, J. & Samec, Z. Effect of water solubility in organic solvents on the standard Gibbs energy of ion transfer across a water/organic solvent interface. *Electrochim. Acta* **449**, 142222 (2023).
72. Heyrovský, J. *Electrochemistry at the Interface between Two Immiscible Electrolyte Solutions (IUPAC Technical Report). Pure Appl. Chem* vol. 76 (2004).
73. Holze, R. Schmickler, Wolfgang; Santos, Elizabeth: Interfacial Electrochemistry, 2nd ed. *Journal of Solid State Electrochemistry* **15**, 855–856 (2011).
74. A. J. Parker. SOLVATION OF IONS-ENTHALPIES, ENTROPIES AND FREE ENERGIES OF TRANSFER. *Electrochemica Acta* **21**, 671–679 (1976).
75. Wilke, S. & Zerihun, T. Standard Gibbs energies of ion transfer across the water 2-nitrophenyl octyl ether interface. *Journal of Electroanalytical Chemistry* **515**, 52–60 (2001).
76. Navalpotro, P. *et al.* Critical aspects of membrane-free aqueous battery based on two immiscible neutral electrolytes. *Energy Storage Mater.* **26**, 400–407 (2020).
77. Navalpotro, P., Ibañez, S. E., Pedraza, E. & Marcilla, R. A neutral pH aqueous biphasic system applied to both static and flow membrane-free battery. *Energy Storage Mater.* **56**, 403–411 (2023).
78. Alcantara, M. L. *et al.* Tuning biphasic electrolytes for membrane-free redox flow batteries: influence of sodium thiocyanate on partition and viscosity. *J. Mol. Liq.* **439**, 128767 (2025).
79. Navalpotro, P., Ibañez, S. E., Pedraza, E. & Marcilla, R. A neutral pH aqueous biphasic system applied to both static and flow membrane-free battery. *Energy Storage Mater.* **56**, 403–411 (2023).
80. Barker, A. L., Unwin, P. R. & Zhang, J. Measurement of the forward and back rate constants for electron transfer at the interface between two immiscible electrolyte solutions using scanning electrochemical microscopy (SECM): Theory and experiment. **3**, 372–378 (2001).
81. Wei, C., Bard, A. J. & Mirkin, M. V. Scanning Electrochemical Microscopy. 31. Application of SECM to the Study of Charge Transfer Processes at the LiquidLiquid Interface. *J. Phys. Chem* **99**, 16033–16042 (1995).
82. Wojeicchowski, J. P. *et al.* Computer-aided design of membrane-free batteries using conductor-like screening model for real solvents. *J. Energy Storage* **72**, 108584 (2023).

83. de Sousa, R. P. F. *et al.* Formulation and study of an environmentally friendly microemulsion-based drilling fluid (O/w) with pine oil. *Energies (Basel).* **14**, en14237981 (2021).
84. Perelomov, L. *et al.* Organoclays Based on Bentonite and Various Types of Surfactants as Heavy Metal Remediants. *Sustainability (Switzerland)* **16**, 4804 (2024).
85. Lu, M., Lindman, B. & Holmberg, K. Effect of polymer addition on the phase behavior of oil-water-surfactant systems of Winsor III type. *Physical Chemistry Chemical Physics* **26**, 3699–3710 (2023).
86. Racovita, R. C., Ciuca, M. D., Catana, D., Comanescu, C. & Ciocirlan, O. Microemulsions of Nonionic Surfactant with Water and Various Homologous Esters: Preparation, Phase Transitions, Physical Property Measurements, and Application for Extraction of Tricyclic Antidepressant Drugs from Aqueous Media. *Nanomaterials* **13**, 2311 (2023).
87. Leng, K. *et al.* Advance of Microemulsion and Application for Enhanced Oil Recovery. *Nanomaterials* **14**, 1004 (2024).
88. Schulz, E. N., Schulz, E. P. & Schulz, P. C. Electrochemistry of Surfactants. in *Application and Characterization of Surfactants* (InTech, 2017). doi:10.5772/67975.
89. Priya Moulik, S. & Kumar Rakshit, A. Physicochemisty and Applications of Micro-emulsions. *J. Surface Sci. Technol* **22**, 159–186 (2006).
90. Maximilian pleines. Viscosity-control and prediction of microemulsions. (University of Montpellier, Doctoral thesis, 2018).
91. Hatay, I. *et al.* Hydrogen evolution at liquid-liquid interfaces. *Angew. Chem. Int. Ed.* **48**, 5139–5142 (2009).
92. Hatay, I., Ge, P. Y., Vrubel, H., Hu, X. & Girault, H. H. Hydrogen evolution at polarised liquid/liquid interfaces catalyzed by molybdenum disulfide. *Energy Environ. Sci.* **4**, 4246–4251 (2011).
93. Hirunpinyopas, W., Rodgers, A. N. J., Worrall, S. D., Bissett, M. A. & Dryfe, R. A. W. Hydrogen Evolution at LiquidjLiquid Interfaces Catalyzed by 2D Materials. *ChemNanoMat* **3**, 428–435 (2017).
94. Zhang, X., Hui, L., He, F. & Li, Y. The Interfacial Interpenetration Effect for Controlled Reaction Stability of Palladium Catalysts. *J. Am. Chem. Soc.* **147**, 436–445 (2025).
95. Lehane, R. A. *et al.* Electrosynthesis of Biocompatible Free-Standing PEDOT Thin Films at a Polarized Liquid|Liquid Interface. *J. Am. Chem. Soc.* **144**, 4853–4862 (2022).
96. Siwiec, A., Dusilo, K., Asztemborska, M. & Opallo, M. Electrocatalysis at vegetable oil water interface. *Electrochem. commun.* **161**, 107694 (2024).
97. Piradashvili, K., Alexandrino, E. M., Wurm, F. R. & Landfester, K. Reactions and polymerizations at the liquid-liquid interface. *Chem. Rev.* **116**, 2141–2169 (2016).
98. Pal, N., Alzahid, Y., AlSofi, A. M., Ali, M. & Hoteit, H. Review on Microemulsions for Conformance Improvement Technology: Fundamentals, Design Considerations, and Perspectives. *Energy and Fuels* **37**, 858–875 (2023).
99. Salisu, A. *et al.* Electrochemical performance and microstructure of microemulsion electrolytes for supercapacitors. *J. Mol. Liq.* **442**, 129069 (2026).
100. Balaj, R. V., Xue, W., Bayati, P., Mallory, S. & Zarzar, L. D. Dynamic Partitioning of Surfactants into Nonequilibrium Emulsion Droplets. *J. Am. Chem. Soc.* **146**, 26340–26350 (2024).
101. Peng, J. *et al.* Electron Transfer in Microemulsion-Based Electrolytes. *ACS Appl. Mater. Interfaces* **12**, 40213–40219 (2020).
102. Szymula, M. & Narkiewicz-Michałek, J. The effect of surfactant adsorption at a glassy carbon electrode on electrochemical oxidation of propyl gallate. *J. Appl. Electrochem.* **36**, 455–462 (2006).
103. Peng, J. *et al.* Decoupling Conductivity and Solubility in Electrolytes Using Microemulsions. *J. Electrochem. Soc.* **168**, 080502 (2021).
104. Skyllas-Kazacos, M., Chakrabarti, M. H., Hajimolana, S. A., Mjalli, F. S. & Saleem, M. Progress in Flow Battery Research and Development. *J. Electrochem. Soc.* **158**, R55 (2011).

105. Weber, A. Z. *et al.* Redox flow batteries: A review. *J. Appl. Electrochem.* **41**, 1137–1164 (2011).
106. Liu, Y. & Wu, L. Recent advances of cathode materials for zinc-ion hybrid capacitors. *Nano Energy* **109**, 108290 (2023).
107. Rubenbauer, H. & Henninger, S. Definitions and reference values for battery systems in electrical power grids. *J. Energy Storage* **12**, 87–107 (2017).
108. Spitthoff, L., Vie, P. J. S., Wahl, M. S., Wind, J. & Burheim, O. S. Incremental capacity analysis (dQ/dV) as a tool for analysing the effect of ambient temperature and mechanical clamping on degradation. *Journal of Electroanalytical Chemistry* **944**, 117627 (2023).
109. Viswanathan, V. *et al.* Cost and performance model for redox flow batteries. *J. Power Sources* **247**, 1040–1051 (2014).
110. Elgrishi, N. *et al.* A Practical Beginner's Guide to Cyclic Voltammetry. *J. Chem. Educ.* **95**, 197–206 (2018).
111. Batchelor-Mcauley, C. & Compton, R. G. Voltammetry of multi-electron electrode processes of organic species. *Journal of Electroanalytical Chemistry* **669**, 73–81 (2012).
112. Levitt, M. H. *Spin Dynamics Basics of Nuclear Magnetic Resonance Second Edition*. (John Wiley & Sons, Ltd, 2008).
113. Sethio, D., Bopp, P. & Hermansson, K. 7Li NMR Chemical Shifts in Battery-Relevant Electrolytes: Ligand-Induced Shifts Cancel in Both Experiment and Calculation. *ChemSusChem* **18**, e202500798 (2025).
114. Veeraraghavan, S. NMR Spectroscopy and Its Value: A Primer. *J. Chem. Educ.* **85**, 537–540 (2008).
115. Simpson, A. J., Simpson, M. J. & Soong, R. Nuclear magnetic resonance spectroscopy and its key role in environmental research. *Environ. Sci. Technol.* **46**, 11488–11496 (2012).
116. Bloch, F. Nuclear Induction. *Physical Review* **70**, 460–475 (1946).
117. Hemminga Marcus A. Introduction to NMR. *Trends Food Sci. Technol.* **3**, 179–186 (1992).
118. Gerothanassis, I. P., Troganis, A., Exarchou, V. & Barbarossou, K. NUCLEAR MAGNETIC RESONANCE (NMR) SPECTROSCOPY: BASIC PRINCIPLES AND PHENOMENA, AND THEIR APPLICATIONS TO CHEMISTRY, BIOLOGY AND MEDICINE. *CHEMISTRY EDUCATION: RESEARCH AND PRACTICE IN EUROPE* **3**, 229–252 (2002).
119. Wong, K. C. Review of NMR Spectroscopy: Basic Principles, Concepts and Applications in Chemistry . *J. Chem. Educ.* **91**, 1103–1104 (2014).
120. Johans, C., Behrens, M. A., Bergquist, K. E., Olsson, U. & Manzanares, J. A. Potential determining salts in microemulsions: Interfacial distribution and effect on the phase behavior. *Langmuir* **29**, 15738–15746 (2013).
121. Meija, J. *et al. Principles of Instrumental Analysis*. *Pure and Applied Chemistry* vol. 88 (Walter de Gruyter GmbH, 2016).
122. Ríos-Reina, R. & Azcarate, S. M. How Chemometrics Revives the UV-Vis Spectroscopy Applications as an Analytical Sensor for Spectralprint (Nontargeted) Analysis. *Chemosensors* **11**, 8 (2023).
123. Zhang, D., Wang, R. (John), Wang, X. & Gogotsi, Y. In situ monitoring redox processes in energy storage using UV–Vis spectroscopy. *Nat. Energy* **8**, 567–576 (2023).
124. Shravani S. More, S. S. M., Sandhya P. Kadam, S. P. K. & Dr. Vivekkumar K.Redasani, Dr. V. K. R. A Comprehensive Review of UV-visible spectroscopy. *International Journal of Pharmaceutical Research and Applications* **10**, 114–134 (2025).
125. Tuna, A., Abbasi, V., Kvarnström, C. & Peljo, P. Unveiling novel capacity (electro)recovery for Chloranilate-based alkaline redox flow batteries. *Journal of Electroanalytical Chemistry* **986**, 119081 (2025).
126. Katano, H., Tatsumi, H. & Senda, M. Ion-transfer voltammetry at 1,6-dichlorohexane|water and 1,4-dichlorobutane|water interfaces. *Talanta* **63**, 185–193 (2004).
127. Jin, S. *et al.* Polarizable potential window at soft molecular interfaces as a quantitative descriptor for the water content in organic solvents. *Chem. Sci.* **16**, 5017–5027 (2025).

128. Trojánek, A., Mareček, V., Fiedler, J. & Samec, Z. Origin of the correlation between the standard Gibbs energy of ion transfer and the solubility of water in organic solvents. *Electrochim. Acta* **465**, 142966 (2023).
129. Vladimirova, E., Peljo, P. & Girault, H. H. Solvent effect in photo-ionic cells. *Journal of Electroanalytical Chemistry* **816**, 242–252 (2018).
130. Jetmore, H. D., Anupriya, E. S., Cress, T. J. & Shen, M. Interface between Two Immiscible Electrolyte Solutions Electrodes for Chemical Analysis. *Anal. Chem.* **94**, 16519–16527 (2022).
131. Peljo, P., Smirnov, E. & Girault, H. H. Heterogeneous versus homogeneous electron transfer reactions at liquid–liquid interfaces: The wrong question? *Journal of Electroanalytical Chemistry* **779**, 187–198 (2016).
132. Smirnov, E., Peljo, P., Scanlon, M. D. & Girault, H. H. Gold Nanofilm Redox Catalysis for Oxygen Reduction at Soft Interfaces. *Electrochim. Acta* **197**, 362–373 (2016).
133. Gamero-Quijano, A., Herzog, G., Peljo, P. & Scanlon, M. D. Electrocatalysis at the polarised interface between two immiscible electrolyte solutions. *Curr. Opin. Electrochem.* **38**, 101212 (2023).
134. Girault, H. H. Electrochemistry at the interface between two immiscible electrolyte solutions. *Electrochemica Acta* **32**, 383–385 (1986).
135. Smirnov, E., Peljo, P., Scanlon, M. D. & Girault, H. H. Interfacial Redox Catalysis on Gold Nanofilms at Soft Interfaces. *ACS Nano* **9**, 6565–6575 (2015).
136. Aydogan Gokturk, P. *et al.* The Donnan potential revealed. *Nat. Commun.* **13**, 5880 (2022).
137. Thomas A. Zawodzinski. Water Uptake by and Transport Through Nafion | 117 Membranes. *J. Electrochem. Soc.* **140**, 1041 (1993).
138. Doyle, M., Lewittes, M. E., Roelofs, M. G., Perusich, S. A. & Lowrey, R. E. Relationship between ionic conductivity of perfluorinated ionomeric membranes and nonaqueous solvent properties. *J. Memb. Sci.* **184**, 257–273 (2001).
139. Sanginov, E. A., Evshchik, E. Y., Kayumov, R. R. & Dobrovol'skii, Y. A. Lithium-ion conductivity of the Nafion membrane swollen in organic solvents. *Russian Journal of Electrochemistry* **51**, 986–990 (2015).
140. Manzanares, J. A., Johans, C. & Cervera, J. Distribution potential in electrified microemulsions with potential determining salts. *Journal of Electroanalytical Chemistry* **819**, 78–86 (2018).
141. Badenhorst, W., Kuldeep, N., Manzanares, J. A. & Murtomäki, L. Unexpected Behavior of Streaming Potential in Ion-Exchange Membranes. *Langmuir* **40**, 7512–7519 (2024).
142. Fang, T. *et al.* Sensing the Potential of Zero Charge at Soft Microinterfaces via Collisional Ionosomes. *Anal. Chem.* **97**, 10208–10217 (2025).
143. Ai-Fariss, T. F., Fakeeha, A. H. & Ai-Odan, M. A. Flow of Oil Emulsion Through Porous Media. *J. King Saud Univ* **6**, 1–16 (1994).
144. Tagavifar, M., Xu, K., Jang, S. H., Balhoff, M. T. & Pope, G. A. Spontaneous and Flow-Driven Interfacial Phase Change: Dynamics of Microemulsion Formation at the Pore Scale. *Langmuir* **33**, 13077–13086 (2017).
145. Hu, Y. *et al.* Pore-scale numerical simulation of in situ microemulsion formation and enhanced oil recovery in porous media. *Front. Chem.* **13**, 1601086 (2025).
146. Zhang, H., Xu, B. & Zhang, H. Mesoscopic simulation on the microemulsion system stabilized by bola surfactant. *J. Dispers. Sci. Technol.* **43**, 1444–1452 (2022).
147. Pommella, A., Caserta, S., Guida, V. & Guido, S. Shear-induced deformation of surfactant multilamellar vesicles. *Phys. Rev. Lett.* **108**, 138301 (2012).
148. She, Y. *et al.* Three-dimensional visualization of the alkaline flooding process with in-situ emulsification for oil recovery in porous media. *J. Pet. Sci. Eng.* **202**, 108519 (2021).
149. Dongqi, W., Daiyin, Y., Junda, W., Yazhou, Z. & Chengli, Z. Influencing factors and microscopic formation mechanism of phase transitions of microemulsion system. *J. Pet. Explor. Prod. Technol.* **12**, 2735–2746 (2022).

150. Kumar, N. & Mandal, A. Surfactant Stabilized Oil-in-Water Nanoemulsion: Stability, Interfacial Tension, and Rheology Study for Enhanced Oil Recovery Application. *Energy and Fuels* **32**, 6452–6466 (2018).
151. Lipfert, F., Kerscher, M., Mattauch, S. & Frielinghaus, H. Stability of near-surface ordering of bicontinuous microemulsions in external shear-fields. *J. Colloid Interface Sci.* **534**, 31–36 (2019).
152. Dongqi, W., Daiyin, Y., Junda, W., Yazhou, Z. & Chengli, Z. Influencing factors and microscopic formation mechanism of phase transitions of microemulsion system. *J. Pet. Explor. Prod. Technol.* **12**, 2735–2746 (2022).
153. Qian, Y. *et al.* Extended Electrochemical Window Via Interfacial Microdomain Regulation by a Bicontinuous Microemulsion-Based Heterogel Electrolyte. *Carbon Energy* **7**, e697 (2025).
154. Jin, S. *et al.* A Water-Miscible Quinone Flow Battery with High Volumetric Capacity and Energy Density. *ACS Energy Lett.* **4**, 1342–1348 (2019).
155. Murata, T., Hamasaki, M. & Morita, Y. A benzoquinone-imidazole hybrid organic anolyte for aqueous redox flow batteries. *Chemical Communications* **60**, 878–880 (2023).
156. Tong, L. *et al.* Molecular Engineering of an Alkaline Naphthoquinone Flow Battery. *ACS Energy Lett.* **4**, 1880–1887 (2019).
157. Kerr, E. F. *et al.* High Energy Density Aqueous Flow Battery Utilizing Extremely Stable, Branching-Induced High-Solubility Anthraquinone near Neutral pH. *ACS Energy Lett.* **8**, 600–607 (2023).
158. Páez, T., Martínez-Cuezva, A., Marcilla, R., Palma, J. & Ventosa, E. Mitigating capacity fading in aqueous organic redox flow batteries through a simple electrochemical charge balancing protocol. *J. Power Sources* **512**, 230516 (2021).
159. Jing, Y. *et al.* In situ electrochemical recomposition of decomposed redox-active species in aqueous organic flow batteries. *Nat. Chem.* **14**, 1103–1109 (2022).

TURUN
YLIOPISTO
UNIVERSITY
OF TURKU

Painosalama, Turku, Finland 2026

ISBN 978-952-02-0697-0 (PRINT)
ISBN 978-952-02-0698-7 (PDF)
ISSN 2736-9390 (Painettu/Print)
ISSN 2736-9684 (Sähköinen/Online)